Konstantinos T. Kleovoulou

Interacting Si Nanocrystals in a-SiO_2: a Monte Carlo study

A Masters Dissertation

Physics Department, University of Crete
Heraklion, Greece
2009

Konstantinos T. Kleovoulou

Interacting Si Nanocrystals in a-SiO_2: a Monte Carlo study

A Dissertation
Submitted to the Physics Department, University of Crete in partial fulfilment of the requirements for the Degree of Master of Philosophy in Physics

Heraklion, Greece, July 2009

Interacting Si Nanocrystals in a-SiO_2: a Monte Carlo study

Thesis author: Konstantinos T. Kleovoulou

Thesis supervisor: Prof. Pantelis C. Kelires

Thesis committee: P. C. Kelires
N. Flytzanis
P. Tzanetakis

Physics Department, University of Crete
Heraklion, Greece
2009

Thesis Abstract

Silicon nanocrystals (Si-nc) embedded in amorphous dielectric matrices (a-SiO_2) have attracted considerable attention both for their fundamental properties and potential applications in Si-based optoelectronic and quantum computing devices. It is particularly a very interesting subject to realize ordered Si-nc assemblies (quantum dot photonic crystals or two-dimensional superlattices). For such an aim, it is necessary to control both the size of Si-nc and their inter-particle distances and positioning/ordering. Despite its importance, a lot of issues concerning the inter-particle interaction of Si-nc still remain unclear.

We present here results of Monte Carlo simulations which shed light onto these issues. In our approach, the generation of the embedding a-SiO_2 structure is achieved via a modified Wooten-Winer-Weaire method. Starting from crystalline beta-cristobalite, the network is amorphized through bond-breaking and switching moves. The Si-nc is positioned at the center of the cell. The energies are calculated using the Keating-like potential. Bond-conversion moves of the type Si-Si to Si-O-Si, and vice versa, allows us to study interdiffusion in the system. A 3.0 nm Si-nc is chosen for our simulations. Through the periodic boundary conditions the inter-particle distance of the nc vary from 0.5 to 4.0 nm.

The energetics, stability and mechanical properties of embedded Si-nc in a-SiO_2 and their variations versus the inter-particle distances are examined. We have shown that the interface properties of Si-nc are strongly influenced by the embedding amorphous oxide matrix. We especially find that the interfacial energy decreases with the variation of the interparticle distance, indicating higher stability of the entire nanocomposite system. There is also indication for preferential ordered arrangements of Si nanocrystals at optimum distances. Large deformations were observed, with the deviations in bond angles to be the dominant contributor to the strain energy. Our findings might play a crucial role in understanding and optimizing the PL properties of ordered Si-nc assemblies.

Acknowledgments

I would like to express my gratitude to my supervisor Prof. P. C. Kelires whose expertise, understanding, and patience, added considerably to my graduate experience. He has been a real mentor to me, without his support I would not have finished this dissertation. Immense thanks should be given to my family. Their love and support they provided me through my entire life was of immeasurable value to me. I also feel the need to thank many other people who helped me while I was working this dissertation. In particular, I must acknowledge G. Hadjisavvas for being good colleague and also a good friend. His support and assistance were catalytic for the completion of this dissertation. Special thanks go to M. Konstantinou for standing by me in the difficult times, and for the encouragement and the editing assistance she offered me. Last but not least, I would like to thank all my friends for being so patient and for their support throughout my academic years.

Contents

Chapter 1

What's past is a prologue
William Shakespeare

1. Silicon Nanocrystals (Si-nc)

1.1 Introduction

What is a Nanocrystal? Nanocrystals (nc) also known as quantum dots are semiconductors. Namely, they are a unique class of semiconductors because their size is of the order of a few nanometers to a few hundred nanometers. At these small sizes materials behave differently giving quantum dots unprecedented tuning ability and enabling never before seen applications to science and technology. The usefulness of nc comes from their peak emission frequency's extreme sensitivity both from the nc size and composition, which can be controlled using engineering techniques. This remarkable sensitivity is due to the ability of the nc to confine electron, holes or electron-hole pairs so called excitons. Nanocrystals confine excitons in all three spatial dimensions. Other quantum confined semiconductors include, quantum wires which confine electrons or holes in two spatial dimensions and allow free propagation in the third, and quantum wells which confine electrons or holes in one dimension and allow free propagation in the other two spatial dimensions.

The electrons in quantum dots have a range of energies. The concepts of energy levels, bandgap, conduction and valence band still apply. However there is a major difference; excitons have an average physical separation between the electron and the hole referred to as the *Exciton Bohr Radius* (E.B.R.), this physical distance differs for each material. In bulk the dimensions of the semiconductor crystal are much larger than the E.B.R allowing the exciton to extend to its natural limit. However if the size of the semiconductor crystal becomes small enough that it approaches the size of the materials E.B.R., then the electron energy levels can no longer be treaded as continuous-they must be treated as discrete. This situation of discrete energy levels is called *Quantum Confinement* (Q.C.) and under these conditions the semiconductor material ceases to resemble bulk and instead can be called a quantum nanocrystal. This feature has large repercussions on the absorptive and emissive behavior of the semiconductor material.

Quantum dots provide a mean to create artificial potentials for carriers, electrons and holes in semiconductors at length scales where confinement takes place. Beside the fundamental point of view semiconductor nanostructures have a large potential for applications in nanoelectronics and optoelectronics. This is because by using the confinement effect new device concepts become feasible which provide additional degrees of freedom in design. Thus quantum mechanics becomes applicable not only in systems of academic interest but also in systems of practical impact.

1.2 Preparation methods and conditions

Silicon nanocrystals have been produced via several different techniques. These include high-dose Si implantation in SiO_2 [1,2,3], laser ablation [4,5], gas evaporation [6], sputter deposition [7,8], low-energy cluster beam deposition (L.E.C.F.D.) [9], plasma-enhanced chemical vapor deposition (P.E.C.V.D.) of sub-stoichiometric Silicon oxide (SiO_x) [10] and even annealing of SiO_x thin film [11]. All of them have their own advantages and disadvantages. The main aim of these methods is to achieve the control of the size profile of the nc. Hence, among these techniques, ion implantation is one of the most suitable choices, giving distributions of nc sizes with width of about 0,6 nm (at half width).

On the other hand, the samples were characterized by different techniques such as infrared spectroscopy, atomic force microscopy (A.F.M.), Scanning Tunneling Microscopy (S.T.M.), high-resolution transmission electron microscope (H.R.T.E.M.), Rutherford backscattering spectrometry (R.B.S.), x-ray absorption spectroscopy (X-A.S.), etc. Again, just as in the case of preparation methods, each technique has its own characteristics. It should be noted that, currently, H.R.T.E.M. is the tool used to image individual Si-nc. However, it is not necessarily the best imaging technique, when quantitative and statistical measurements have to be performed. Also, the poor contrast between Si and SiO_2 makes the measurements extremely difficult. Note that nc with diameter of less than 1.0 nm are very difficult to be distinguished from the SiO_2 matrix [12]. In this size regime, the nc consists of about four planes of atoms.

1.3 Sample Characteristics

The various techniques and experimental conditions used to prepare these systems, give samples with different chemical, structural and optical properties. As a consequence, the interpretation of the light emission mechanism, given in different works, is often controversial mainly due to the lack of accurate sample characterization. Important information concerns the amount of Si atoms segregated in the Si-nc, the evaluation of the size and distribution of the clusters. The chemical composition and structure of the interface (and even the host matrix) are also crucial parameters. However, the actual structure of the amorphous matrix depends on Si concentration, deposition parameters, and annealing treatments. The Silicon total content in most samples varies from 35 to 46 %.

The main findings are summarized below:

- It is known that silicon si-nc exhibit strong photoluminescence (PL) in the red, when their sizes are in the range of 3 to 5 nm. Also, the PL energy shifts to larger wavelengths, when the mean size increases.

- Some times, PL is not immediately observable after the preparation of the sample. It takes from few hours to few days until the luminescence becomes clearly visible. This effect is believed to correlate with the progressive oxidation of the surface. So, by increasing the compositional ratio of oxygen, the PL peak wavelength blueshifts, due to the size reduction of the nc.

- It has been demonstrated that the luminescence signal from the nc, increases by increasing the annealing temperature. Moreover, the luminescence peak position slightly redshifts by increasing the temperature of thermal annealing.

- Silicon nanocrystals are actually surrounded by some sub-stoichiometric silicon oxide (SiO_x, $x<2$) transition "amorphous" layer [13]. It has also been shown that the thickness of this amorphous layer increases by increasing the size of the nc, always representing approximately 10% of the total diameter [14].

1.4 Previous theoretical work

Silicon nanocrystals embedded in amorphous dielectric matrices attracted great attention the past years from many theoretical groups, moreover three different systems related to the Si-nc/a-SiO_2 nanocomposite system have been studied until now. The first system is the planar interface of Si/a-SiO_2, which revealed structural and chemical information about the interface. The second system is the free-standing (isolated) Si-nc terminated by either Oxygen (O) or Hydrogen (H). These systems were mainly used in order to understand the optical properties of the nc. The third system is Si-nc embedded in crystalline silicon dioxide (c-SiO_2) which gives results on both structural and optical properties. Finally some aspects of the Si-nc/a-SiO_2 system have been studied including energetics, optical properties and the nature of the structure. Especially much attention was given to the morphology and composition of the non planar interface of such a system.

1.4.1 Planar interface

Much effort [15, 16, 17, 18] has been devoted to the understanding of the planar Si(001)/a-SiO_2 interface. It is found that the lowest energy structural element is a bridge bond. A bridge bond is a Si-O-Si bond connecting two Si atoms on the surface of the substrate. These bonds can bend and stretch with minimal energy cost. The structure with the lowest interface energy is found to be an abrupt transition between the Si substrate and the a-SiO_2. More specifically, two very close energetically structures are the most favorable ones, the check and stripe phase. Both of them consist of fully bridge-bonded structures. These two structures are shown in Fig. 1.1.

The existence of bridge bonds has been verified using Monte Carlo simulations by Tu and Tersoff [19]. The level of the bridge bonding reached by these simulations was of the order of ~75 %. Bridge bonds are also found by *ab initio* calculations to be the lowest structural elements. Furthermore, it is shown that an interface with no suboxide layers (an abrupt transition) has lower energy than an interface with suboxides. [17]. The a-SiO_2/Si interface widths reported in literature range from abrupt to more than 0.7 nm wide. These variations may reflect different preparation conditions. However, it is quite clear that various measurements techniques probe different aspects of the interface. For example, many methods can't resolve the atomic structure but some average. Other techniques require intrusive sample

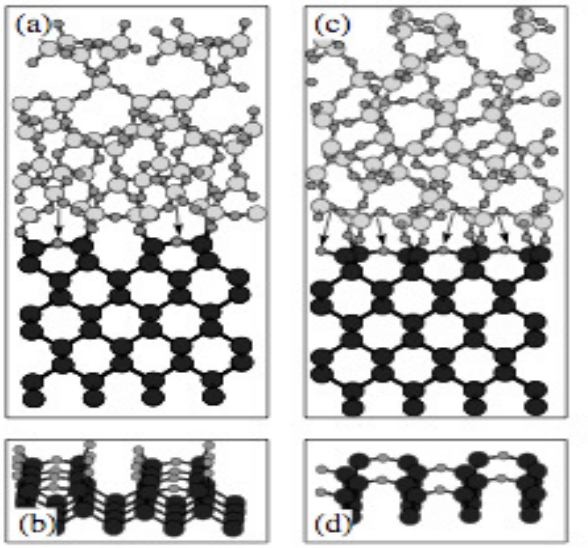

Fig. 1.1: Planar interface Si(100)/a-SiO2. Two very close energetically structures stripe (a), (b) and check (c), (d) phase. Arrows indicate bridge bonds. The black (light grey) balls represent Silicon (Si) atoms in substrate (a-SiO_2) while smaller light gray balls represent oxygen (O) atoms.

preparation methods, such as depth profiling by sputtering or etching, which alter the chemistry of the interface.

For the a-SiO_2/Si(111) interface it is shown that the suboxide states, including Si^{1+}, Si^{2+} and Si^{3+}, exhibit different depth distributions. Using a simple model, which is based on the statistical cross-linking of dangling bonds between the Si substrate and the amorphous silicon dioxide chemically abrupt interface is proposed [20]. The a-SiO_2/Si(100) interface is far more important for device applications and far more suitable for theoretical investigation than the a-SiO_2/Si(111) counterpart. Indeed extensive theoretical studies were performed for the a-SiO_2/Si(100) interface. Most of them suggested a chemically graded interface with the suboxide distributed over a range of about 0.6nm [21,22]. More specifically, it is known that the Si^{1+} and Si^{2+} species have the same depth distribution, while the Si^{3+} species are distributed in a wider region from the interface boundary. In more detail, it is suggested that there are three transition layers. The distribution of the suboxides at each transition layers are 36% Si^{1+} and 64% Si^{2+}, 71% Si^{3+} and 29% Si^{4+}, and 35% Si^{3+} and 65% Si^{2+}, at the first, second and third interracial layers from the substrate, respectively [21]. A schematic illustration of the chemical composition of those transition layers is shown in Fig. 1.2.

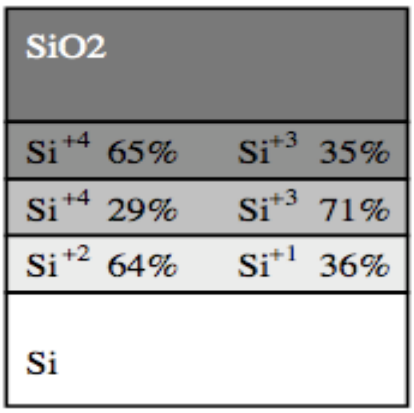

Fig. 1.2: Schematic illustration of the chemical composition of the transition layers based on the model of Ref. [21].

The knowledge however gained from these studies, can't directly be transferred to the case of Si-nc/a-SiO_2 interface which is curved, more or less spherical, and so encompasses all crystal orientations. Most importantly, its bonding and energetics are functions of the nanocrystals size, due to the dramatic change of surface area to volume ratio, a factor which is absent in the planar case.

1.4.2 Isolated Si-nc

On the other hand, most of the work concerning isolated Si-nc, passivated by either O or H, is done in order to explain the opening of the band gap during the reduction of the nc. This is because the observed redshift has been attributed to surface oxidation of silicon nc. It is believed that Oxygen creates trapped electron and hole states on noncrystalline surfaces. In Fig.1.3.a an isolated Si-nc passivated by H is shown. Different models have been proposed. The group of Ossicini [23] considered the role of the surface geometry distortion of small hydrogenated Si cluster in the excited state. More specifically, they studied the case of Hydrogen incorporation into a strained Si-Si bond, revealing a lowering in transition energies by 1.1 to 1.2 eV. In this way, they pointed out that distortions should no longer be neglected.

On the other hand, some groups reported that the oxidation introduces defect levels in the silicon Si-nc band gap, pinning their emission energy. These defect levels were due to the formation of Si=O double bonds so called "silanone" [24, 25]. A nc which is passivated by H and has one Si=O double bond is shown in Fig 1.3.b. Finally, Vasiliev et al [26] have pointed out that similar results can be obtained also for O connecting two Si atoms (Si-O-Si bridge bonds) at the Si-nc surface. An example of bridge bond is illustrated in Fig.1.3.c. All these findings give us the opportunity to conclude that either bridge bonds or double bonds are responsible for the reduction of the band gap. However, those simulated systems ignore the structural changes, which might be induced on both the surface and the inner parts, when the nc are embedded in the amorphous oxide.

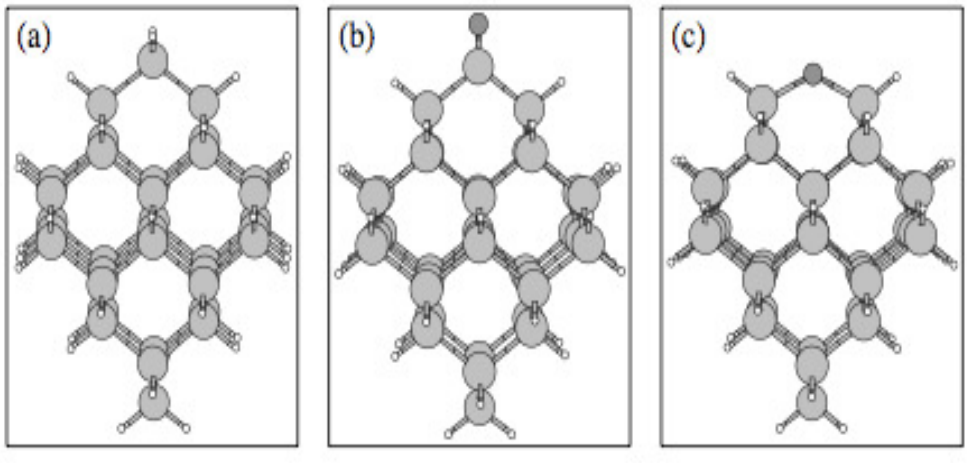

Fig. 1.3: Three different types of isolated Silicon nanocrystals (Si-nc) passivated with Hydrogen (H). In panel **(a)** the nanocrystal is terminated only with Hydrogen (H) ($Si_{35}H_{36}$), in **(b)** has one Si=O double bond ($Si_{35}OH_{34}$), and in **(c)** has one Si-O-Si bridge bond ($Si_{34}OH_{34}$). The light gray atoms stand for Silicon (Si), the white ones for Hydrogen (H) and the dark gray for Oxygen (O).

1.4.3 Si-nc/c-SiO_2

In one of the very few previous theoretical attempt to simulate the structure of the Si-nc/c-SiO_2 interface [27], a crystalline SiO_2 embedding matrix was used (beta-crystobalite). In this case, the core of the Si-nc is of crystalline nature, while the interface, between Si-nc and SiO_2, extends on a transition layer of about 1.0 nm width. Moreover, the structure of this region is progressively changing from the crystalline core to amorphous Silicon, to stressed SiO_2, and finally to c-SiO_2. An illustration of the studied structure is shown in Fig.1.4. The two dashed circles help to highlight the three different regions in which the final relaxed structure is organized. The inner region indicates the strained Si-nc, while between the dashed lines is a cap shell of distorted b-SiO_2 around the nc. In the outer region is shown the crystalline b-SiO_2. The optical properties of this system are compared to experimental data, revealing that not only Si-nc, but also modified silica capping region plays an important role. Although this attempt eases the computational load, it is not accurate representation of the real situation. Nevertheless, this study represents only the first step towards our complicated models closer to the real samples.

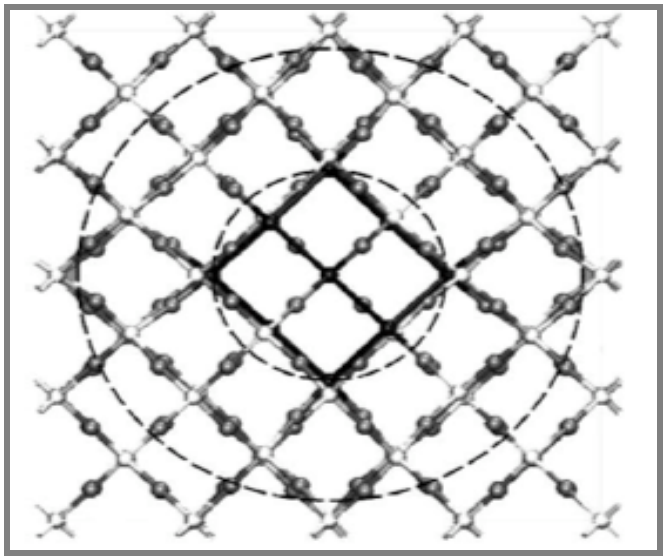

Fig. 1.4: Top view of the relaxed structure for the Si_{10}/b-SiO_2 supercell. The white and the gray balls stand for the Silicon (Si) and Oxygen (O) atoms of b-SiO_2, the black ones for the Silicon (Si) atoms of the nanocrystal.

1.4.4 Si-nc/a-SiO_2

Silicon nanocrystals embedded in an amorphous silicon dioxide matrix (a-SiO_2) is a very promising system currently under intense investigation. Such a system has superior quality and stability with respect to porous silicon (p-Si).

Various scientific groups carried out a lot of work in the interpretation and manipulation of the energetics and unique electronic properties of such a nanocomposite system. Major attention has been given to the investigation of the energetics, stability and disorder as a function of the nc size. In order to interpret the results taken out from these investigations one is lead to examine firstly the interface between the nc and the host matrix.

Of great importance is the string between the interface complexion and the whole system taking into account aspects like the kind and proportion of bonds, the width of the interface and the silicon oxidation states. As for the shape of the interface comparison with the much studied planar one, provided a mean to understand the impact of spherical shaped nanocrystals to the nanocomposite system.

A very important finding by Kelires and Hadjisavvas [28], who for the first time simulated Si-nc in a realistic amorphous SiO_2 matrix, was that a large number of bridge bonds Si-O-Si has been formed on the interface, with a relative fraction of ~60%. The formation of bridge bonds on the interface was due to the need of lower interfacial strain energy. As it was previously mentioned bridge bonds have been found to be the lowest structural elements. The relative fraction of ~60% found by [28] remarkably approaches the one of ~75% found by Tu and Tersoff [19] in their study on the planar interface. Another important feature of the nanocomposite system, given light by [28] was the distribution of suboxide components at the interface. They found that Si^{2+} is concentrated at the interface, Si^{1+} is found toward the Si-nc and Si^{3+} occurs mainly toward the host matrix and this comes with agreement to the findings of [19] again on their study of the planar interface. Moreover Djurabekova and Nordlurd [29] found that the relative number of suboxide atoms was close to the one of dangling bonds (a dangling bond occurs when an atom is missing a neighbor). In their finding Si atoms with one dangling bond is the most common coordination defect and finally the ratio between coordination defects and suboxide atoms varies with the annealing temperature. It is assumed that by increasing the annealing temperature the ratio mentioned before changes and this is due to the fact that some coordination defects eventually turn into suboxides. Different aspects of the impact coming from the variation of the Si-nc size were studied by different groups. Kelires and Hadjisavvas [28] came across to the fact that by decreasing the size of the Si-nc it looses its crystallinity and the whole nanocomposite system has lower stability. What actually occurs is that the interfacial energy increases by shrinking the Si-nc, for Si-nc of diameter ~2,5-5 nm the rise in interfacial energy of the ideal planar Si(001)/a-SiO_2 interface with no suboxide layers (lower limit) and the energy of the planar interface with suboxide layers (upper limit). For Si-nc of diameter less than 2nm the interfacial energy rises sharply (Fig. 1.5).

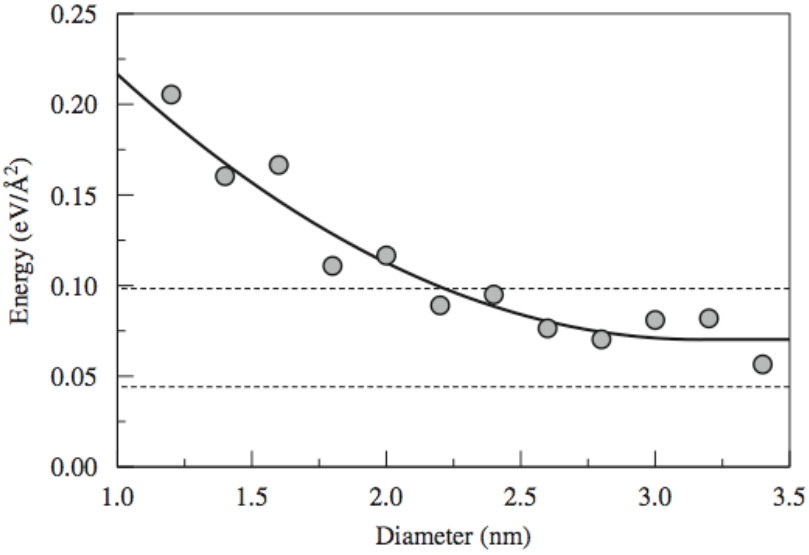

Fig. 1.5: Variation of interface energy with the Si-nc size. Solid line is a fit to the points. The dashed horizontal lines denote the energy of the planar interface without suoxides(bottom) and with suboxides (top). Figure is taken from Ref. [28].

Moreover it was found by [29] that the bigger size of Si-nc stabilizes the interface constraining it in a thinner region. The relative number of coordination defect almost does not vary with the size of the Si-nc, [29] find it to be ~10% of the total number of interface atoms. On the other hand L. Colombo et al. [30] found that a fair amount of strained Si-Si and Si-O bonds exist in the interface, some stretched and other compressed from their normal length in bulk. This deviation in bond length decreases with the increase of the nanocrystals size and this feature plays a role in the increase of the stability of the whole system. The analysis on the interface complexion revealed the presence of Si=0 bonds so called “silanone bonds” which are known to be important for the optical properties of Si-nc/SiO_2 structures. The presence though of such bonds is very limited i.e. only one in the whole interface was observed. Despite the big attention given in the size of the Si-nc almost none was given to the responce of such a nanocomposite system in the variation of interparticle distance. The aim of this dissertation is to create the means needed, and study how any change in the distance between Si-nc affects the stability and energetics of this unique nanocomposite system.

Chapter 2

Μη είναι βασιλικήν ατραπόν επί γεωμετρίαν

Ευκλείδης

2. Methodology

2.1 The method of Wooten - Winer - Weaire (W.W.W.)

Construction of amorphous materials has been a subject of great attention given by various scientific groups over the past years, hence there exist a plethora of techniques and models which can be used for this purpose.

However the question subject gets even more difficult to deal with due to the unique characteristics of amorphous structures, such as the fact that from practical experience we know that models consisted of hundreds of atoms are needed in order to get adequate information on the properties of such a structure, and the fact that the models have to conform to periodic boundary conditions in order to avoid free surface problems. The method of W.W.W. meets the above criteria hence considered to be one of the most elective methods for the construction of amorphous networks. The method of W.W.W. originally developed for generating amorphous silicon (a-Si) networks. Remarkably though with minor changes, it can be easily used for construction of a-SiO_2 networks so called silica. The idea is, to start from a crystalline silicon dioxide supercell that conforms to periodic boundary conditions and to perform an amount of rearrangements so that structures amorphization will be finally achieved. According to Wooten et al. [31] such kind of rearrangements must not produce excessive bond distortion. The exact procedure of such a rearrangement is as follows.

Initially a pair of nearest neighbors is chosen at random (atoms 1 and 5 in Fig. 2.1). Then two first neighbors, one for each of the referred to above atoms are chosen (atoms 3 and 8 in Fig. 2.1) .The latter choice though must follow some restrictions.

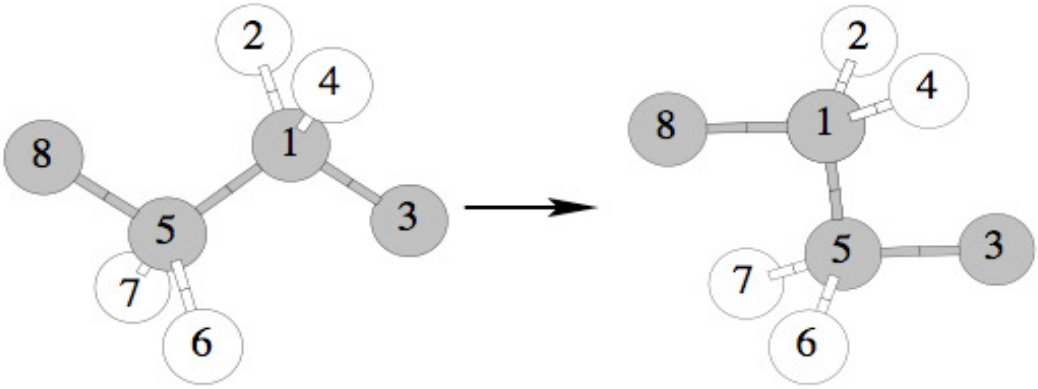

Fig. 2.1: A bond switch move. The elementary rearrangement applied by Wooten et al. [31].

Firstly the bonds between the atoms of the initial pair and their first neighbors must be as parallel as possible. This criterion can be met by choosing the first neighbors not

to be part of any five, six or seven-fold rings. Moreover atoms that belong to four-fold rings can't be chosen either, since they cause large distortion to the length of the bonds. For high annealing temperatures though the latter can be chosen due to the expectation that such rings will vanish during the annealing procedure. Secondly the bond length must not be too large, namely rearrangements for bond length greater than 1.7 of the desired one can't be done. When the proper choice of neighbors is been done the bond between the initial atoms and their first neighbors is broken and a new bond connecting one of the initial atoms and the others neighbor is created. As it is illustrated in Fig 2.1 the spatial positions of the atoms has to be change and as a result the system becomes strained, though the tetrahedral nature of the structure is preserved. This change of first neighbors is called "bond switch move".

The rearrangement of the final structure varies with the amount of bond breaking and switching moves. Moreover excessive use of such moves could lead to structures were almost every characteristic of the initial diamond structure has been vanished. Such a structure has rms bond angle deviation of 22º which is two times bigger than the desired one. The moves have to be followed by geometrical configuration which minimizes the energy of the whole system in order to achieve a realistic model with the proper rms bond angle deviation. The above geometrical configuration can be done by estimating the power between the atoms and bringing them topologically to their equilibrium positions. The estimate of the power between the atoms can be done by using Keating empirical potential [32]. If the structure is not sufficiently randomized then the imposition of the requirement that all further rearrangements must lower the energy will result a return to the structure of crystalline silicon dioxide that we started from. In some cases even the most perfectly randomized structures could turn bag to the initial structure but in most cases they just find their way into a metastable state, where no bond switch can lower the energy. The problem with this metastable state is that it has an rms bond angle deviation of 13º or more, few degrees more than the experiment suggests. The solution to this problem is to include a Maxwell-Boltzmann factor $e^{-E/K_\beta T}$ which occasionally lifts the structure out of the metastable state and allows it to find a lower energy amorphous state. In practice, two bonds are switched at random and the end the energy difference between the initial and the final structure is calculated

$$\Delta E = E_f - E_i \qquad (2.1)$$

If the new structure has lower energy than the one of the change, is accepted otherwise it is accepted with probability $e^{-\Delta E/K_\beta T}$ where k_B is the Boltzmanns constant and T is the temperature. This approach is of course the Metropolis algorithm [33] applied to optimization by simulated annealing.

A lot of improvements for the method of W.W.W. have been introduced since then. Some of them really speed up the calculation time, while others were practical only for rare cases. Here, we used two modifications by Barkema and Mousseau [34] which were useful in our case. The improvements introduced are the following:

- First, the evaluations of the acceptance of the trial move using the Metropolis accept/reject procedure was done without doing full relaxation of the supercell. In order to do so, we have to decide first a threshold energy which is given by

  $$E_t = E_b - k_B \, T \ln(s) \qquad (2.2)$$

  where s is a random number between 0 and 1, E_b is the initial energy of the structure before the bond rearrangement. Since the energy is harmonic around the

minimum, the decrease in energy obtained during further relaxation is approximately equal to the square of the force times some proportional constant c_f. So, during the relaxation the final energy can be estimated to be:

$$E_f \approx E - c_f |F|^2 \quad (2.3)$$

where E is the energy of every relaxation step. In this way, if at any moment during the relaxation, $E - c_f |F|^2$ is greater than the threshold energy E_t the trial move is rejected. We must note that the note c_f depends on the units and the system which is applied. In our case c_f is well below 1. Also to account for unharmonicities, the moves are not rejected during the first steps of the relaxation. Using this modification a lot of computational time is gained from the moves, which are eventually rejected, producing a more efficient method

- A local/nonlocal relaxation procedure is used. It is presumable that the atoms with large strain are those close to the bond switch. So, instead of the whole cell, the three neighbours are limited gaining again a lot of computational time. In combination with the previous improvement, this makes the time per bond rearrangement almost independent of the configuration size.

Interfaces between Si and a-SiO_2, such as planar interfaces or even Si nanocrystals embedded in a-SiO_2, cannot compositionally equilibrate only with bond switch moves. One is thus led to introduce another type of moves, which are called bond conversion moves. This type of moves is shown in Fig. 2.2 In this scenario a Si-Si bond is exchanged with a Si-O-Si and vice versa. Note that the number of Si and O atoms remains constant, thus we do not have to use any chemical potential. However, the method can be generalized to allow fluctuations in the number of atoms of each species (semi-grand ensemble), in order to study nucleation, clustering, expansion of nanocrystals, and other phenomena. Also, applying this type of move interdifusion in the system is allowed to be studied.

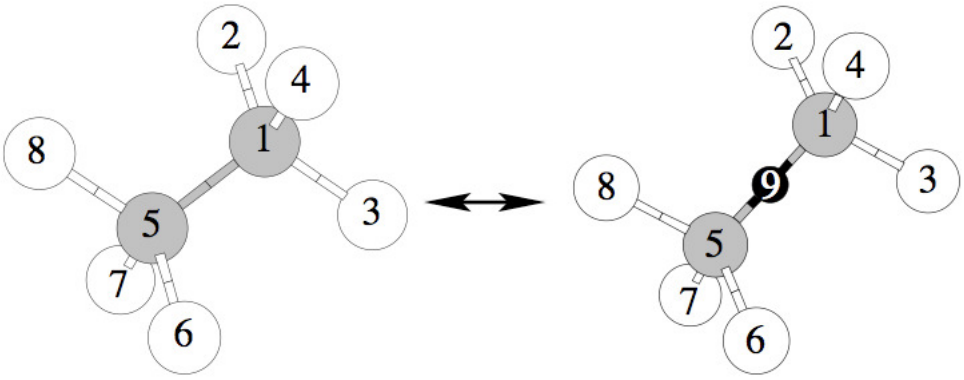

Fig. 2.2: A Bond conversion move, introduced by P. C. Kelires and G. C. Hadjisavvas, a Si-Si bond is changed with a Si-O-Si bond and vice versa. The total number of atoms is preserved.

2.2 Empirical potentials

A good classical potential is one that with a small number of free parameters can describe a wide range of properties well and is also "transferable". The latter means that it should be able to describe properties of other states of the material than those it was fitted to. The parameters are determined by a fitting procedure, so as to reproduce various physical quantities of the references system. Some of the properties which are used to fit interatomic potentials are crystal structure, cohesive energy, elastic constants, equation of state P(V), neutron scattering, etc.
A classical potential can be written in the form:

$$V = \sum_i V_1(r_i) + \sum_{i,j} V_2(r_i, r_j) + \sum_{i,j,k} V_3(r_i, r_j, r_k) + \ldots \qquad (2.4)$$

where:

- V is the total potential energy of an N atom system. In principle all sums loop from 1 to N while in practice they can often be much reduced in order to gain computational time.
- V_1 is the single particle potential, which describes external forces (e.g. an electric field). In system with no external forces this part is 0.
- V_2 is a pair potential which only depends on the distance between atoms $r_{ij} = |\bar{r}_i - \bar{r}_j|$. Note that if there were the direct dependence on the vectors $\bar{r}_i, \bar{r}_j$ (and not on their difference), the potential would depend on the choice of the origin. In many cases, an environment dependence is embedded into the two-body term, as we will see later.
- V_3 is a "three-body potential: which may have an angular dependence. To preserve the independence on the atom indices, the potential has to depend only on three variables, i.e. $V_3 = V_3(r_{ij}, r_{ik}, \theta_{ijk})$.
- Four-body and even five-body potentials do exist, especially in chemical and biological applications. The potentials we are interested in are up to three-body term.

2.2.1 Keating-like Potential

The empirical potential which we use is Keating –like [32]. This valence force model depends on both the positions $\{\bar{r}\}$ of atoms and the set of bonds connecting pairs of atoms. It is simple three body term potential and its functional form is:

$$E_{\{\bar{r}\}} = \tfrac{1}{2}\sum_i k_b(b_i - b_0)^2 + \tfrac{1}{2}\sum_{i,j} k_\theta(\cos\theta_{ij} - \cos\theta_0)^2 + \gamma\sum_{m,n}(d_2 - |\bar{r}_m - \bar{r}_n|)^3 + U \qquad (2.5)$$

The first two terms represent the cost of bond-length and bond-angle distortions, respectively. The third term is used to ensure that the neighbor atoms will be included in the neighbor list and distant atoms will be excluded. So, *m* and *n* label atoms which are neither 1st nor 2nd neighbors, but for which $|\bar{r}_m - \bar{r}_n|$ is actually less than the

distance $d_2 = 3.84\,\text{Å}$ between next-nearest neighbors in crystalline Silicon. Also, parameter $\gamma = 0.5\,eV/\text{Å}^3$ [35, 19] and the term *U* represents a "suboxide penalty", the chemical energy cost for the of any suboxide, taken by *ab initio* calculations [36]. Here *i* and *j* represent the i_{th} and j_{th} bond of the network while *m* and *n* represent atoms. The parameters of the potential are given summarized in Table 2.1.

Table 2.1: Parameters of the Keating-like potential for Silicon and Oxygen.

	k_b	b_o		k_θ		$\cos\theta_0$		U
Si-Si	9.08	2.35	Si-Si-Si	3.58	Si	-1/3	Si^{1+}	0.47
Si-O	27.0	1.60	O-Si-O	4.32	O	-1.00	Si^{2+}	0.51
			Si-Si-O	3.93			Si^{3+}	0.24

2.3 The Monte Carlo Method – The Metropolis Algorithm

2.3.1 The Monte-Carlo Method

The Monte Carlo (MC) method is a powerful numerical approach for the approximate solution of complex mathematical problems using sampling techniques. In its most basic application, it is used for the numerical integration of high-dimensional integrals or for the calculation of averages over a multivariable probability distribution. Standard numerical methods involve the discretization of the integration range into a regular grid and sampling of the integrand over it. In MC method instead of using such a grid, N random numbers in the integration range are taken, x_t and the mean value, M, of the integrated function f(x) is calculated. In this way the integral will simply be I = L M where L is the integration length and

$$M = \frac{1}{N}\sum_{i=1}^{N} f(x_i) \quad (2.6)$$

In order to achieve better precision in MC integration the process of sampling is modified to reduce the variance of the function without altering the mean value. This is the concept of the importance sampling which is tightly connected with the MC method. Importance sampling is choosing a good distribution from which to stimulate ones random variables. It involves multiplying the integral by 1 (usually dressed up in "tricky fashion") to yield an expectation of a quantity that varies less than the original integrand over the region of integration. For example let w(x) be a density for the random variable x which takes values only in L so that

$$\int_{X\in L} W(x)dx = 1 \quad (2.7) \qquad \text{Then} \qquad \frac{W(x)}{W(x)} = 1 \quad (2.8)$$

$$\text{and} \quad \int_{X\in L} f(x)\,dx = \int_{X\in L} f(x)\frac{W(x)}{W(x)}dx \quad (2.9)$$

$$W(x_i)P_{ij}(x_i \to x_J) = W(x_j)P_{ji}(x_j \to x_i) \quad (2.10)$$

A simple choice for the transition probability could easily be:

$$P_{ij}(x_i \rightarrow x_j) = \min\left[1, \frac{W(x_j)}{W(x_{i)}}\right] \quad (2.11)$$

The theoretical basis for MC simulations is the theory of *Markov process.* Suppose we have a discrete sequence of random variables $x_1,x_2,x_3,\ldots$ that take values in a finite state space S(N) of N states, generated such as that the next state x_{n+1} depends only on the current state x_n and not on the previous one. A Markov chain is the set on the successive states generated Markov process, starting from an initial state. The probability $P(i \rightarrow j)$. Of course the transition probabilities must satisfy the conditions of *positivity* and *normalization*.

$$P(i \rightarrow j) \geq 0 \quad (2.12)$$

and

$$\sum_{j=1}^{M} P(i \rightarrow j) = 1, \quad \forall i \quad (2.13)$$

The Markov process is chosen in a way that when the simulation runs long enough, every state *i* will be passed with a frequency proportional to a desired probability distribution π_i In order to produce this distribution starting from any initial state, some conditions should be also satisfied. The first one is the *ergodicity condition* which implies that Markov process any state *j* in state space must be accessible by any other state *i*. The second one is called the *balance condition*. The condition ensures that after the period of time needed for the Markov process to reach the desired distribution, the probability of occurrence of any state in the Markov chain should not change in time. Finally the *detained balance condition* says that the Markov process on average should pass from state *i* to state *j* as often as it passes from state *j* to state *i*, for any pair of state *i*, *j*.

2.3.2 The Metropolis Algorithm

The Metropolis Algorithm is a technique to create a Markov chain over some state space, which converges to a desired probability distribution π_i. This algorithm can be

$$P(i \rightarrow j) = \min(1, \frac{\pi_j}{\pi_i}) \quad (2.14)$$

very easily used in any ensemble, as it will be shown. As it is mentioned this scheme should satisfy the condition of ergodicity and balance condition. In this way the choice of Metropolis et al. for the transition probability was:

The main steps of the Metropolis algorithm are shown below:

1. Initial configuration of the system

2. Choose randomly an atom

3. Move it r > r´
4. Compute the difference of the potential $\Delta W = W(\bar{r}') - W(\bar{r})$
5. If ΔW<0 accept the move and continue to step 2.
6. Compute $p = e^{-\beta \Delta W}$
7. Pick a random number h(0,1)
8. If h<p keep configuration and go to step 2
9. Reject it and go to step 2

where the potential ΔW is tightly connected with the transition probability π_i which was used above. It depends of the ensemble which is used. In the next section we will see all the ensembles used in our simulation and how this potential changes in each one.

2.4 Non Crystalline Materials

Non crystalline materials, otherwise known as amorphous, are materials whose structure lacks long-range crystalline periodicity, i.e., the pattern of it constituent atoms or molecules does not repeat periodically in three dimensions in a long range. Though the positions of the atoms are not completely random like in gases but there exist a sort range periodicity.

Formerly it was believed that only a number of elements or compounds could be in amorphous state. These days it is proven that any liquid can be cooled into an amorphous solid. As it is shown in Fig. 2.3 a liquid can be cooled into a solid since cooling reduces molecular mobility. If the cooling rate is faster than the rate at with molecules can organize into a more thermodynamically favorable crystalline state then an amorphous solid will be formed. In contrast if molecules have sufficient time to organize into a structure with two or three dimensional order then a crystalline (or semi-crystalline) solid will be formed.

Hence in order for a liquid to become amorphous solid the cooling rate must fall from T_f (temperature of crystallization) to T_g (glass transition temperature) very fast. Temperature value T_g varies for different materials. Amorphous materials can also be produced by additives which interfere with the ability of the primary constituent to crystallize.

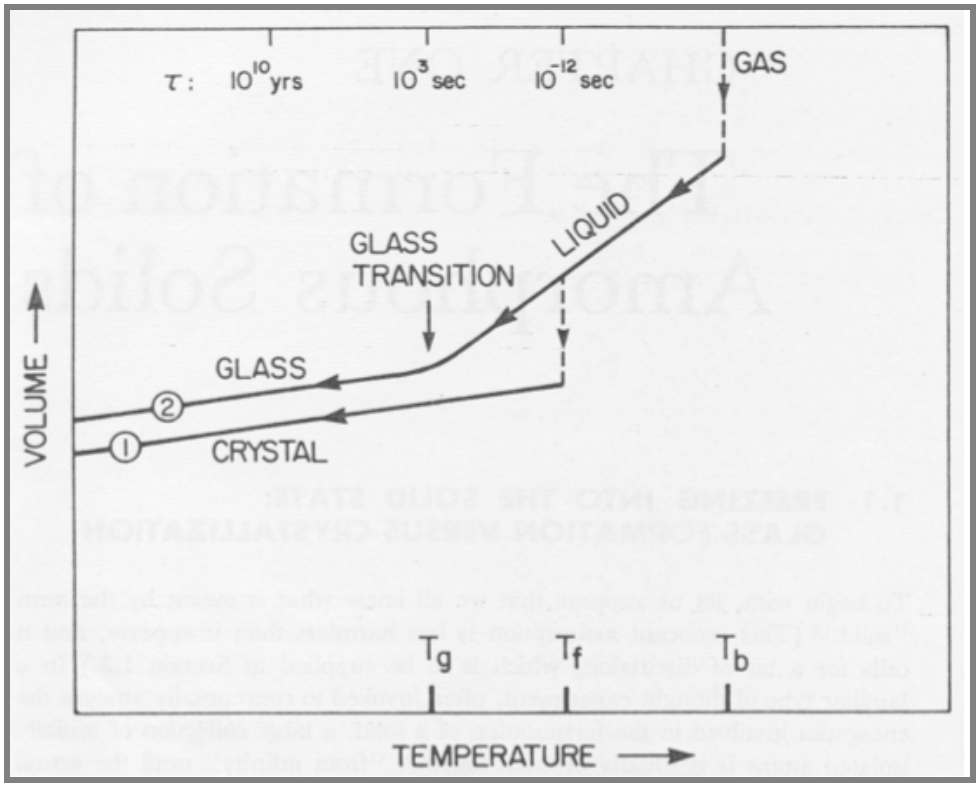

Fig. 2.3: The two general cooling paths by which an assembly of atoms can condense into the solid state. Route (1) is the path to the crystalline state, route (2) is the rapid quench path to the amorphous solid state.

As it was previously stated the main difference between crystallize and amorphous materials is that the latter lacks in crystalline periodicity. This absence of periodicity is not entire like in gases. In gases, the position of an atom has no correlation with the position of other atoms so what one observes is a complete random arrangement of the atoms as it is shown in Fig. 2.4.c. In amorphous materials an absence of long range periodicity is observed, so randomness could come across in long distances though in short scale, like in the distances of first neighbors, there exist an order in the positions of the atoms. In crystalline solids any atom has a fixed position in the material even for long distance from the observation point as it is illustrated in Fig. 2.4.a. This short-range periodicity for amorphous or long-range for crystalline solids is due to the kind of the bond that holds the solid.

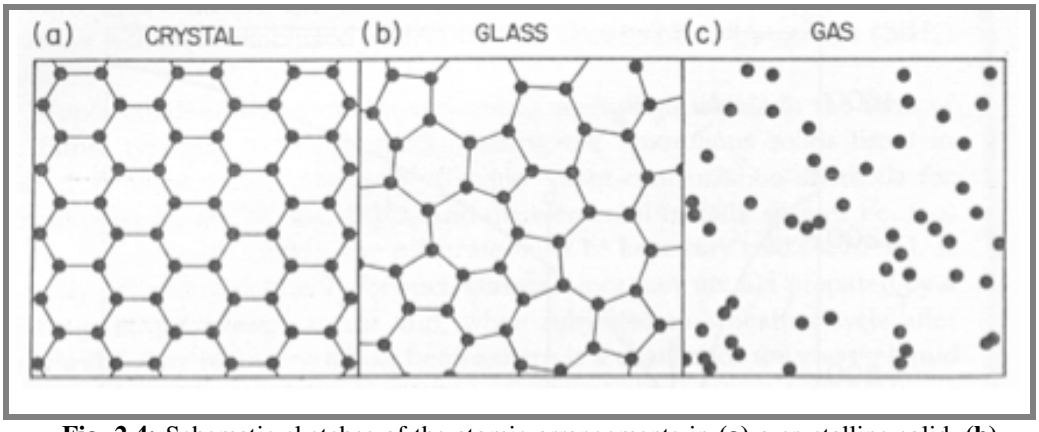

Fig. 2.4: Schematic sketches of the atomic arrangements in **(a)** a crystalline solid, **(b)** an amorphous solid, and **(c)** a gas.

2.4.1 Silicon dioxide

Silicon dioxide, also known as silica, is one of the most commonly encountered substances in both daily life and in electronics manufacturing. It has a number of distinct crystalline forms in addition to amorphous forms, it is an important constituent of a great many minerals and gemstones, both in pure form and mixed with related oxides. Beach sand is mostly silica. The working of silica into glass has been known since antiquity, with polished glass lenses in eyeglasses and optical instrument dating back more than five centuries. Silica in the amorphous form is a dielectric material. It is a network that suffers from short range crystalline periodicity just as all amorphous materials do. Each atom in the amorphous solid has the same number of covalent bonds as in their crystalline phase, the amorphous nature of the structure is reflected by the random network made by the covalent bonds. An illustrative picture of an amorphous silicon dioxide is shown in Fig. 2.6. The whole of planar electronics processing and the modern industry has been made possible by the unique properties of silicon dioxide, the only native oxide of a common semiconductor which is stable in water and at elevated temperatures, an excellent electrical insulator, a mask to common diffusing species, and capable of forming a nearly perfect electrical interface with its substrate.

Silicon dioxide is formed by strong, directional covalent bonds, and has a well-defined local structure: four oxygen atoms are arrayed at the corners of tetrahedron around a central silicon atom as it is illustrated in Figure 2.5.

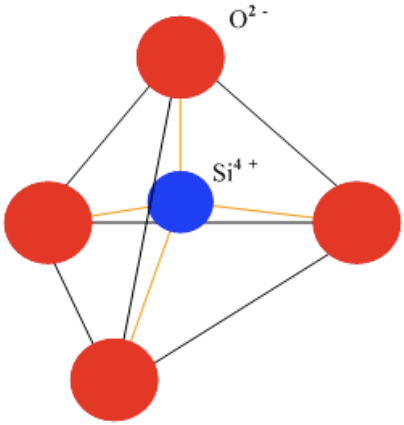

Fig. 2.5: Silicon oxygen tetrhendron. The angle between to Si-O atoms is found to be 109º47´.

Table 2.2: Important properties of pure silicon dioxide:

Density	2.0-2.3 gm/cm^3
Electrical conductivity	Varies widely
Breakdown field	>1E7 V/cm in thermal oxides; can be as low as 1E6 V/cm in CV_d oxides
Thermal conductivity	0.01W/cm K (bulk)
Thermal diffusivity	0.009 cm^2/sec (bulk)
Coefficient of thermal expansion	0.5 ppm/K [note Si thermal exp(2.3) ppm/K]

Silicon dioxide has a number of distinct crystalline forms in addition to amorphous forms. With the exception of Stishovite and fibrous silica, all of the crystalline forms involve tetrahedral SiO_4 units linked together by shared vertices in different arrangements. Silicon-oxygen bond lengths vary between the different crystal forms and so is the Si-O-Si angle. (see Table 2.2) Stishovite, the highest pressure form, in contrast has a rutile like structure where silicon is sixfold coordinate. The density of is stishovite $4.287 g/cm^3$, which compares to a-quartz, the densest of the low pressure forms, which has a density of $2.648 g/cm^3$. The difference in density can be ascribed to be increase in coordination as the six shortest Si-O bond lengths in Stishovite (four Si-O bond lengths of 176 pm and two others of 181 pm) are greater than the Si-O bond length (161 pm) in a-quartz. The change in the coordination increases the ionicity of the Si-O bond. Note that the only stable from under normal conditions is a-quartz and this is form in which crystalline silicon dioxide is usually encountered.

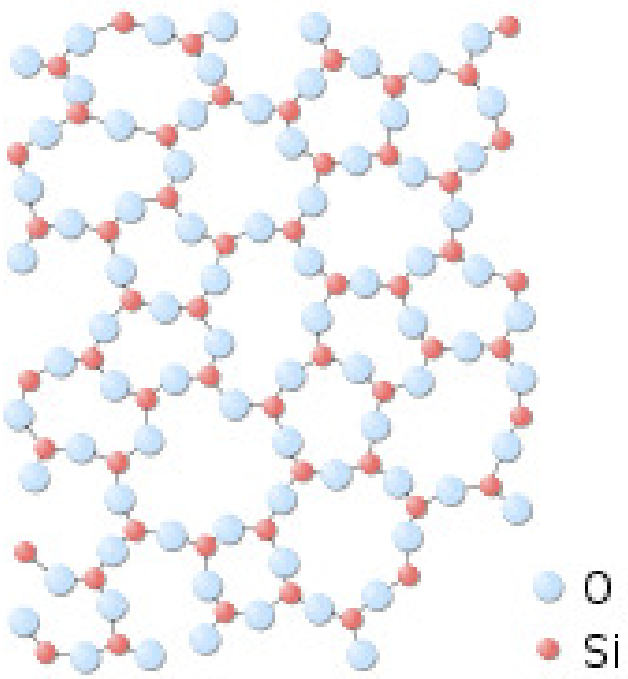

Fig. 2.6: The amorphous network of silicon dioxide. The tetrahedral character is preserved though there exist only short scale periodicity

Table 2.3: Crystalline forms of SiO_2

Form	Crystal Class	Structural features	Notes
a-quartz	rhombohedral (trigonal)	Helical chains making individual single crystals optically active	a-quartz converts to β-quartz at 573 ºC
b-quartz	Hexagonal	Closely related to a-quartz (with an Si-O-Si angle of 155º)and optically active	β-quartz converts to β-tridymite at 870 ºC
a-tridymite	Orthorhombic	Metastable form under normal pressure	
b-tridymite	Hexagonal	Closely related to a-tridymite	β-tridymite converts to β-cristobalite 1470 ºC
a-cristobalite	Tetragonal	Metastable form under normal pressure	
b-cristobalite	Cubic	Closely related to a-cristobalite	melts at 1705 ºC
Keatite	Tetragonal	$Si_5O, Si_4O_{14}, Si_8O_{16}$ rings	synthesized from amorphous silica and alkali at high pressure
Coesite	Monoclinic	Si_4O_8 and Si_8O_{16} rings	High pressure form(higher than keatite)
Stishovite	Tetragonal	rutile like with 6-fold coordinated Si	high pressure form (higher than coesite) and the densest of the polymorphs
Melanophlogite	Cubic	Si_5O_{10}, Si_6O_{12} rings	mineral always found with hydrocarbons in interstitial spaces-a clathrasil
Fibrous	Orthorhombic	like SiS_2 consisting of edge sharing	
Faujasite	Cubic	sodalite cages connected by hexagonal prisms; 12-membered ring pore opening; faujaite structure	

2.5 Bridge Bonds

It is the oxygen "bridge" bonds between silicon atoms that give SiO_2 many of its unique properties. The bond angle Si-O-Si is nominally about 145 degrees, but can vary from about 100 to 170 degrees with very little change in bond energy. Furthermore, rotation of the bond about the axis is almost completely free as it is illustrated in Fig. 2.7

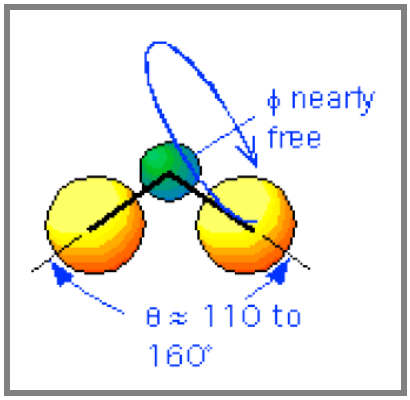

Fig. 2.7: An illustration of a single bridge bond and it's deegres of freedom.

The result of this flexibility in the bridge bonds is that, SiO_2 while it has many different possible crystalline structures, can easily form amorphous materials. The amorphous form of silicon dioxide is a key dielectric material currently used in silicon devices and the basic constituent in the question system Si-nc/a-SiO_2.

Moreover Tu and Tersoff [19], in their study on the Si-nc/a-SiO_2 planar interface using Monte Carlo simulations they find that the interface structure is dominated by Si-O-Si bridge bonds (Figure 2.8.a), the formation of oxygen bridge bonds relaxes most of the strain energy caused by the lattice mismatch between the two materials. Furthermore, they find that the lowest interfacial strain energy state corresponds to the interface structure where oxygen bridge bonds form (2X1) striped pattern (Figure 2.8.b). The level of the bridge bonding reached by these simulations was of the order of ~75%.

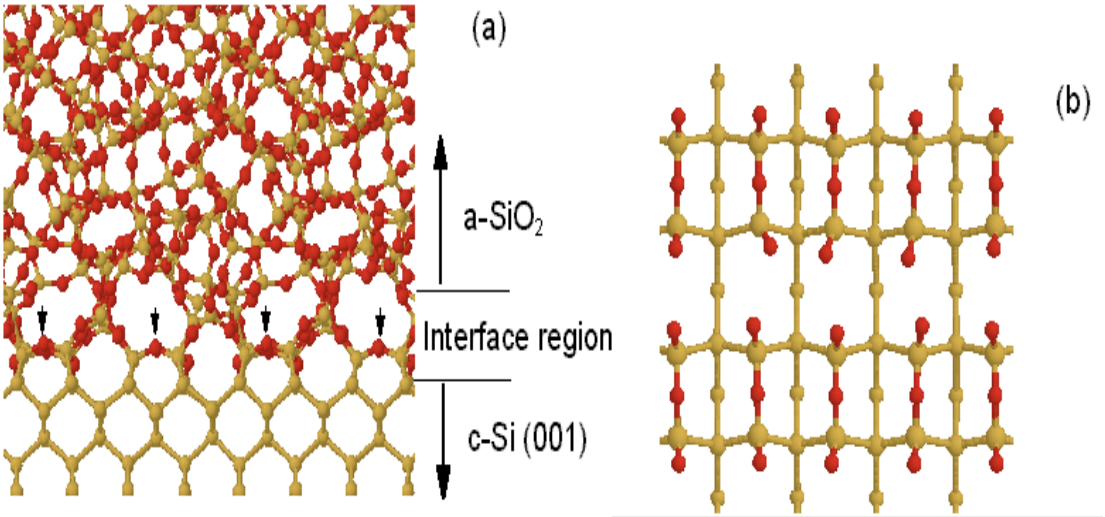

Fig. 2.8: Side view of the a-SiO_2/c-Si(001) interface structure, the arrows indicate the locations of the Si-O-Si bridges.(b) Top viw of the stripe structure of the oxygen bridge bonds at the interface.

2.6 Statistical Ensembles

Statistical physics is concerned with the study of systems composed of a large number of particles, i.e. atoms, molecules, electrons, etc., and thus having many degrees of freedom. Its scope is to relate the microscopic level with the macroscopic one. Let's say we have a classical system in equilibrium. This system is described by the Hamiltonian $H(\bar{r}^N, \bar{p}^N) = K + U$ which is the sum of the kinetic and potential energy of the particles. Here, $\bar{r}$ stands for the coordinates and $\bar{p}$ for the momenta of *N* particles. In this notation, the mean value of every observable quantity $A(\bar{r}^N, \bar{p}^N)$ is given by the sum over all states on the phase space with respect to the stationary probability $P(\bar{r}^N, \bar{p}^N)$:

$$\langle A \rangle = \frac{1}{h^{3N} N!} \int A(\bar{r}^N, \bar{p}^N) P(\bar{r}^N, \bar{p}^N) d\bar{r}_N d\bar{p}_N \quad (2.15)$$

where the factor h^{3N} is introduced because of the quantization of phase space while the factor *N*! appears due to the indistinguishability of identical particles.

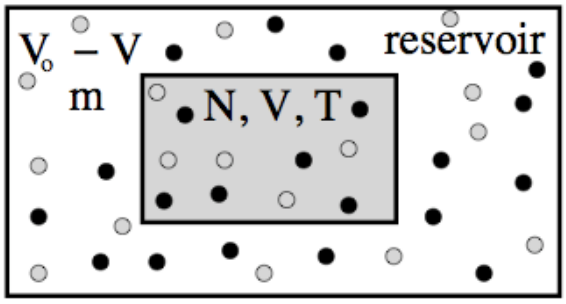

Fig. 2.9: Schematic representation of canonical ensemble. The number of particles, the volume and the temperature of the system are kept fixed (N,V,T).

2.6.1 Canonical ensemble - (N,V,T)

In the case of the canonical ensemble, the quantities which are kept constant are the number of particles, the volume and the temperature of the system, (N,V,T). A schematic representation of this ensemble is shown in Fig. 2.9 in which the system is sketched inside a reservoir. The proper thermodynamic potential, whose minimum determines thermal equilibrium is the Helmholtz free energy

$$F = E - TS = -k_B T \ln Z(N,V,T) \quad (2.16).$$

On the other hand, the probability distribution is

$$P(\bar{r}^N, \bar{p}^N) = \frac{e^{-\beta H(\bar{r}^N, \bar{p}^N)}}{Z(N,V,T)} \quad (2.17)$$

where

$$Z(N,V,T) = \frac{1}{h^{3N}N!}\int e^{-\beta H(\bar{r}^N,\bar{p}^N)}d\bar{r}^N d\bar{p}^N \qquad (2.18)$$

is called the partition function of the system, where k_B is the Boltzmann factor and

$$\beta = \frac{1}{K_B T} \qquad (2.19)$$

.

Applying the above equations in Eq. 2.15 one gets:

$$\langle A\rangle = \frac{\int A(\bar{r}^N,\bar{p}^N)e^{-\beta H(\bar{r}^N,\bar{p}^N)}d\bar{r}^N d\bar{p}^N}{\int e^{-\beta H(\bar{r}^N,\bar{p}^N)}d\bar{r}^N d\bar{p}^N} \qquad (2.20)$$

Note that the Hamiltonian is a quadratic function of momenta, meaning that the integrations with respect to the latter can be carried analytical. On the other hand the integration of functions $A(r^{-N})$, like the potential energy $U(r^{-N})$, over the configuration part of the phase space is the difficult part. In this case the integration over momenta cancel out, and Eq. 2.20 is written:

$$\langle A\rangle = \frac{\int A(\bar{r}^N)e^{-\beta U(\bar{r}^N)}d\bar{r}^N}{\int e^{-\beta U(\bar{r}^N)}d\bar{r}^N} \qquad (2.21)$$

In this ensemble the acceptance probability of a trial move is:

$$P_{acc} = \min(1, e^{-\beta\Delta W}) \qquad (2.22)$$

where:

$$\Delta W = U(\bar{r}'^N) - U(\bar{r}^N) \qquad (2.23)$$

2.7 Analysis Tools

2.7.1 Coordination number

The coordination number z denotes the number of nearest neighbor atoms. For example, z is 4 for the diamond structure, or 12 for the F.C.C. structure. For perfect lattices, the coordination number has no real significance but for more complex structures, like amorphous lattices, it plays a crucial role in the determination of the amorphous structure type. It will be shown in the next section that z for the amorphous material is very close to that of the corresponding crystal. It can be noted that the coordination number may be measured by determining the integrated area under the first peak of radial distribution function. The number of particles located in the region between r_1 and r_2 are:

$$n = \int_{r_1}^{r_2} 4\pi r^2 \rho_0 g(r) dr \qquad (2.24)$$

In the case where r_1=0 and r_2 is such that g(r) = 0, equation 2.24 denotes calculation of the area under the first peak. This area is a direct expression of z.

2.7.2 Radial Distribution Function (R.D.F.)

The Radial Distribution Function R.D.F. is a generalization of coordination number, namely is a type of pair correlation function which describes the density of interatomic distances in a material. In other words R.D.F. describes how on average the atoms in a system are radially packed around each other. This proves to be a particularly effective way of describing the average structure of disordered molecular systems such as amorphous materials (glasses, polymers, liquids).

Experimentally, R.D.F. can be deduced from x-ray or neutron diffraction studies and also light scattering. In a solid the radial distribution function is a sum of delta functions:

$$g(r) = \sum_i z_i(r)\delta(r - r_i) \qquad (2.25)$$

where z(r) is the number of neighbors.

So in the plot of R.D.F. as a function of interatomic separating (Fig. 2.10.a) you can see sharp peaks whose separations and highs are characteristic of lattice structure. In a disordered molecular system a typical R.D.F. plot (see Fig.2.10.b) shows a number of important features. Firstly at short separations (small r) the R.D.F. is zero, this indicates the effective width of the atom. Secondly a number of obvious broadened peaks appear witch is a sign that atoms pack around each other in shells of neighbors. The occurrence of peaks at long range indicates a high degree of ordering.

At high temperature the peaks are broad showing thermal motion while at low temperature they are sharp. At very long range, every R.D.F. tends to value 1 and that happens because R.D.F. describes the average density at this range.

2.7.3 Angular Distribution Function (A.D.F.)

The Angular distribution Function also known as bond angle distribution function, is a type of Root Mean Square Deviation (R.M.S.D.) and is defined for angles between nearest neighbours atoms. For a diamond crystal, g(θ) is a delta function centered at g(θ)=109.47 °. For an amorphous crystal, g(θ) is centered at an angle close to the tetrahedral angle. Significant width of the bond angle distribution indicates large angle distortion. In experiment, the bond angle can be obtained by the ratio of the first and second neighbor distances (r_0 and r_1 respectively) as in

$$\theta = 2\arcsin(r/2r_0) \qquad (2.26)$$

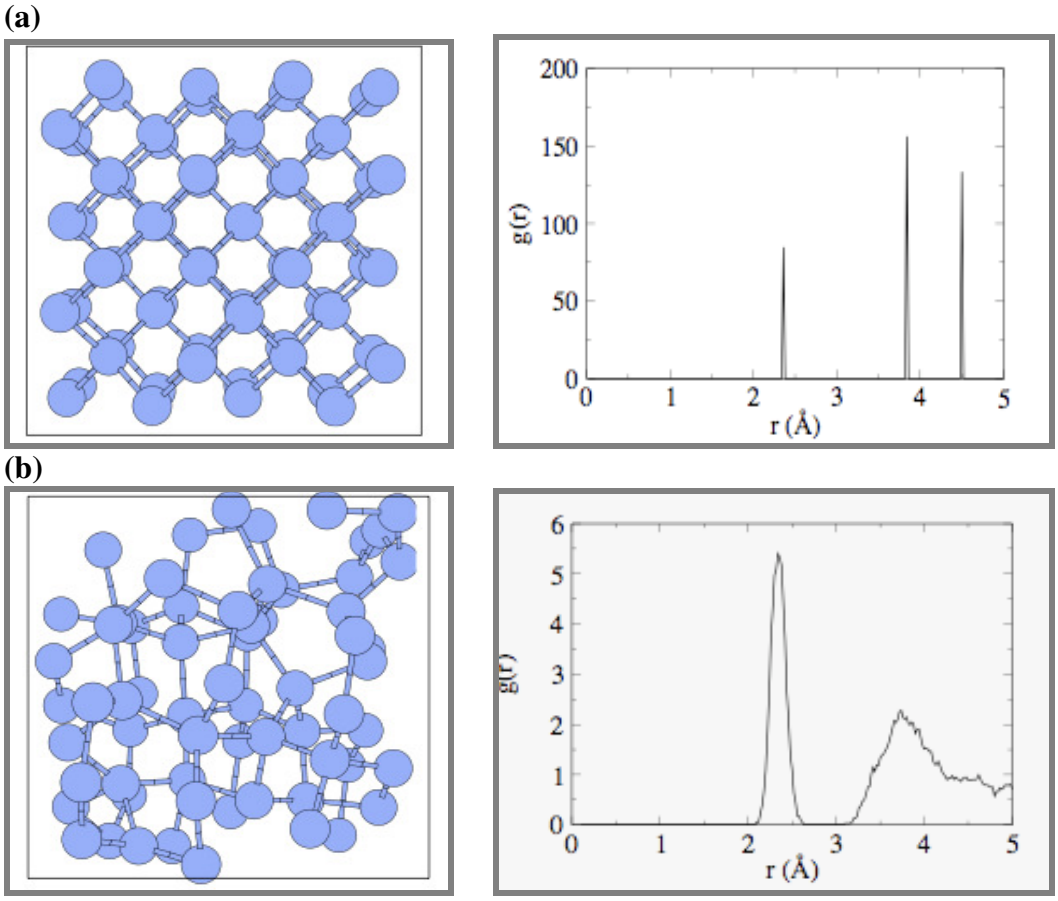

Fig. 2.10: (a) supercell of crystalline silicon (c-Si) and its R.D.F. g(r) consisted of delta functions, **(b)** supercell of disordered system and its R.D.F. g(r) showing the special characteristics

2.7.4 Root Mean Square Deviation (R.M.S.D.)

The root mean square deviation (R.M.S.D.) is a measure of the differences between values predicted by a model or an estimator and the values actually observed from the thing being modelled or estimated. In some cases the R.M.S.D. is used to compare differences between two things that may vary, neither of which is accepted as the "standard" one. For example, when measuring the average distance between two oblong objects, expressed as random vectors

$$\theta_1 = \begin{bmatrix} x_{1,1} \\ x_{1,2} \\ \vdots \\ x_{1,n} \end{bmatrix} \quad \text{and} \quad \theta_2 = \begin{bmatrix} x_{2,1} \\ x_{2,2} \\ \vdots \\ x_{2,n} \end{bmatrix}. \tag{2.27}$$

The formula is:

$$\mathrm{RMSD}(\theta_1, \theta_2) = \sqrt{\mathrm{MSE}(\theta_1, \theta_2)} = \sqrt{\mathrm{E}((\theta_1 - \theta_2)^2)} = \sqrt{\frac{\sum_{i=1}^{n} (x_{1,i} - x_{2,i})^2}{n}}. \tag{2.28}$$

Chapter 3

3. Si-nc embedded in a-SiO_2

3.1 Introduction

Since Canham's discovery of intense light emission in porous Si at the beginning of 1990's [37] great attention was given to the study of Si nanostructures which have improved photoluminescence (PL) efficiency as compared to bulk silicon. Silicon nanocrystals have many advantages compared to the porous Si including high stability, self organized quantum well structure and compatibility with metal-oxide semiconductor technology. Seminal experimental and computational studies on the properties and characteristic of this nanostructures were done and some interesting features of them emerge, such as the opening of the band gap when the nc size decrease [37, 38, 39, 28] and this is due to the quantum confinement of carriers in the three dimensional potential well of the nc.

Of great importance is the role of the interface structure on the behavior of such composite materials. The kind and proportion of bonds, the width of the interface and the Silicon oxidation states are crucial parameters witch have been studied by various scientific groups. Nevertheless, what still remains unclear is the impact on the stability of such nanocomposite system coming from the variation of the interparticle distance. The aim of this dissertation is to shed some light onto this aspect.

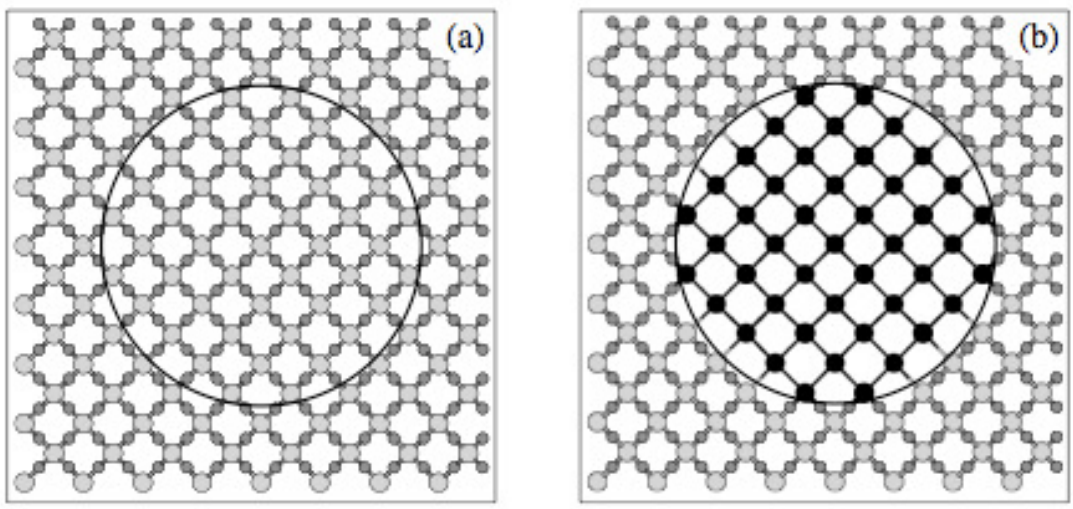

Fig. 3.1: Ball and stick model (part of a thin slice cut) of a Si-nc embedded in a-SiO2. Dark spheres show Si atoms in the nc. Large (small) grey spheres show Si (O) atoms in the oxide, respectively.

3.2 Simulation

In order to study the impact on the system due to the change in the distance between the nanocrystals we alter their ordering by building several models where in each and every one of them the nc are topologically placed in different position.

Computationally, the way for this to happen is to build a cubic cell and generate the nc in the center of it (see Fig. 3.1). Then by increasing the size of the cell in every new model built, but keeping fixed the size of the nc, i.e., increasing the size of the matrix, the distance between the nc and its image due to the periodic boundary conditions is increases also. (See Fig. 3.2.a). In this way a nc cluster is generated via computational methods that can simulate the ones prepared in a lab see (Fig. 3.2.b).

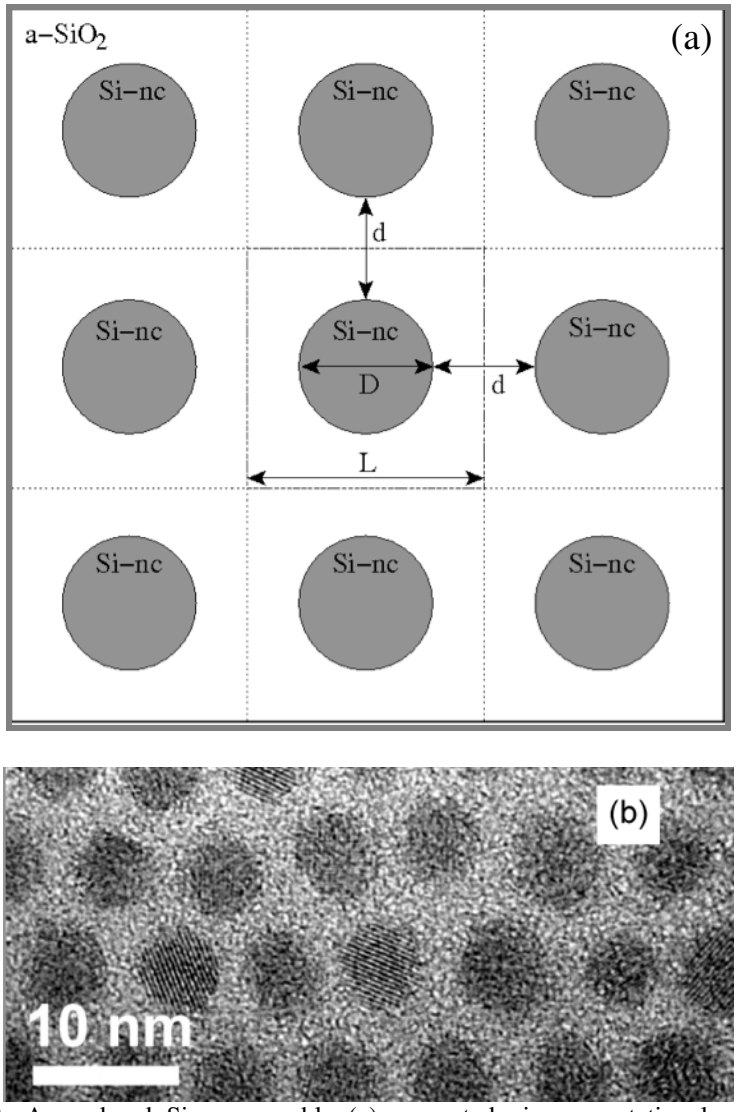

Fig. 3.2: An ordered Si-nc assemble (a) generated via computational method (b) prepared in the lab.

3.2.1 Construction of the cell

The composite system is generated as follows. We start from a cubic cell in the beta-cristobalite structure. The way to obtain such a structure is to start from a cell in the diamond structure, consisting of silicon atoms, and an oxygen atom is interposed in every Si-Si bond. In this way the cubic cell alters into a strained beta-cristobalite structure. A typical cubic cell in the beta-cristobalite structure is shown in Fig. 3.3.

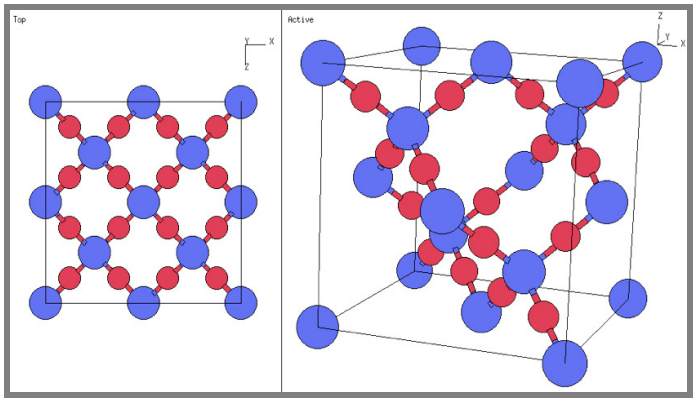

Fig. 3.3: Cubic cell in the beta-cristobalite structure. The cubic cell consists of 16 oxygen atom and 8 Si atoms.

Experiments show that the diameter of the nc is customarily found to be of around 2-5 nm. In order for our simulations to be as much realistic as possible we choose to generate nc of 3nm in diameter. Taking into account that the beta-crystobalite's lattice constant is about 7.16 Å, and that of the diamond structure is about 5.43 Å, we generate a super cell composed of 216 unitary cubic cells (6x6x6). The super cell's acme is 32.58 Å and consists of 5184 atoms. We generate the nc by removing all the oxygen atoms in a radius of 1.5nm from the centre of the cell. Then, this unphysical starting geometry, which is highly strained both in the Si-nc and the crystalline SiO_2 region is relaxed to its energy minimum.

As a result of the topological relaxation the acme of the super cells reaches 37.83 Å though the nc size remains the same. At this point we generated a Si-nc of 3 nm in diameter, embedded in a crystalline SiO_2 host matrix. The next step is the amorphization of the matrix.

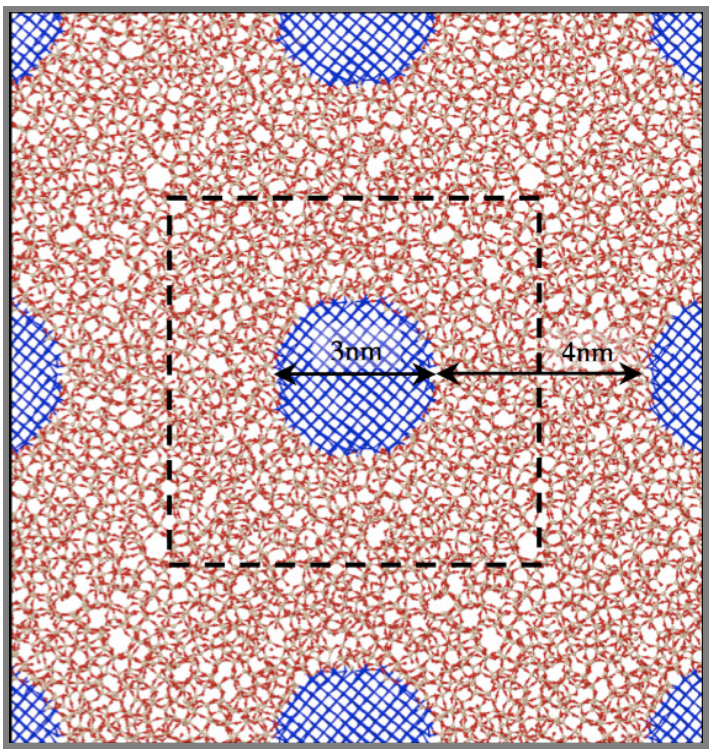

Fig. 3.4: Ball and stick model (part of a thin slice cut) of Si-nc embedded in a-SiO_2 cluster. The doted line denotes the boundaries of the supercell. The interparticle distance is simulated via periodic boundary condition.

3.2.2 Amorphization of the host matrix

To generate the amorphous oxide, the MC algorithm of Wooten, Winer, and Weaire [31] is used. This is a well established method to generate continuous random networks, starting from the perfect crystal, by bond breaking and switching [16, 18, 31]. To compositionally equilibrate the interface, we use bond conversion moves [16], which exchange a Si-Si bond in the nc with a neighboring Si-O-Si bond in the oxide. The number of Si and O atoms remains fixed this way. In both types of moves, we first relax locally the structure, following the attempted move, using a steepest-descent method minimizing the forces on the atoms. Then, the change ΔE in energy between this final and the initial configuration is calculated. The attempted move is accepted or rejected according to the Metropolis criterion. Bond switching and conversion moves are periodically followed by volume relaxation moves to relieve the stress in the entire system.

Particularly we perform MC bond switching in the oxide at a high temperature ($K_\beta T$=3eV) for 40 000 moves, allowing it to liquefy. Subsequently, the temperature is gradually reduced to 0.1 eV, bringing the oxide to its glassy, amorphous state [18]. Quenching lasts for more than 1 000 000 moves. During these processes the positions of the atoms in the Si-nc are kept fixed. We then perform unconstrained MC bond conversion and switching of the entire composite system at 0.1 eV, (887 C) for up to 3 000 000 moves, allowing it to both compositionally and topologically equilibrate.

3.2.3 Results

The same procedure is carried out for the generation of 8 other supercells. The characteristics of the supercells are illustrated in the Table 3.1.

Table 3.1 The characteristics of the supercells

Number of beta-cristobalite cubic cells	***Number of atoms in supercell***	***Number of atoms in nanocrystal***	***Acme of the supercell (nm)***	***Distance between the nanocrystals (nm)***
216 (6x6x6)	3756	705	3.8	0.8
343 (7x7x7)	6852	706	4.6	1.6
512 (8x8x8)	10860	705	5.4	2.4
729 (9x9x9)	16116	706	6.0	3.0
1000 (10x10x10)	22572	708	6.8	3.8
1331 (11x11x11)	30531	705	8.1	5.1
1728 (12x12x12)	41472	705	8.9	5.9

3.3 Structural Characteristics

3.3.1 Interface Energy

The variation of the interface energy, the main indicator of the nanocomposite system's stability, is shown in Fig. 3.5. This energy can be defined as the difference between the total energy, including the suboxide penalty, and the sum of the bulk energies of the amorphous oxide and crystalline Si.

$$E_{for} = E_{tot} - N_{c\text{-}Si}\, E_{c\text{-}Si} - N_{SiO2}\, E_{SiO2} \qquad (3.1)$$

Where: $N_{c\text{-}Si}$ is the number of atoms of the nc.
$E_{c\text{-}Si}$ is the energy per atom of the crystalline silicon.
N_{SiO2} is the number of atoms of the host matrix.
E_{SiO2} is the energy per atom of the amorphous crystalline dioxide.

We observe that the increase of the interparticle distance is followed by a decrease in the interface energy indicating higher stability of the system. Interestingly, there seems to be a minimum in this variation at ~ 3 nm, indicating a preferential ordered positioning of the nc's in the amorphous matrix. However, we still need to calculate the energy at larger interparticle distances, and for nc's of different size, in order to confirm this possibility. To explain this behaviour, we rigorously examine various aspects of the nanocomposite system and we analyse the interracial energy into various contributions.

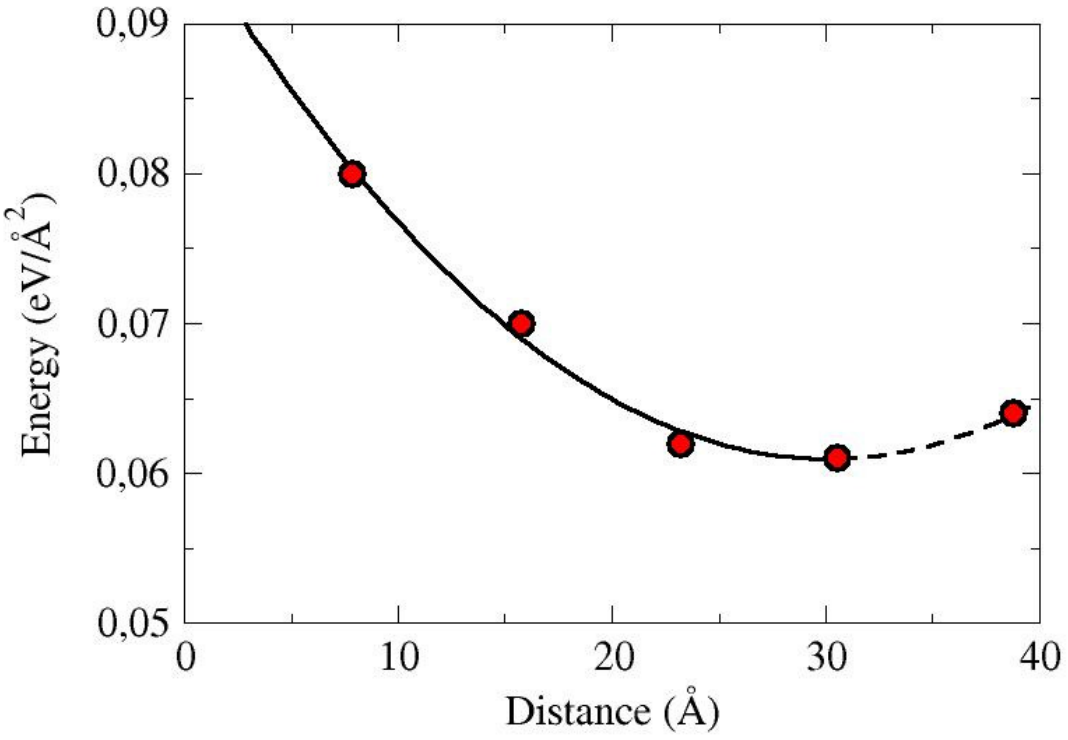

Fig. 3.5: The increase of the interparticle distance is followed by a decrease of the interface energy indicating higher stability of the system.

3.3.2 Bridge Bonds

When it comes to energy decrease the first thing that one should study is the formation of bridge bonds on the interface. As it was repeatedly stated before bridge bonds are the lowest energy structure hence a probable contributor to any change in energy. In our study on the bridge bond formation we realize that the percentage of bridge bond remained almost constant with the variation of the interparticle distance. As it is illustrated in Fig. 3.6, the percentage of silicon atoms participating in a bridge bond versus the interparticle distance is found to fluctuate over ~ 60% of the total silicon atoms of the interface, with a slight tendency to increase for large interparticle distances, showing that bridge bonding had very little to do with the referred increase of stability.

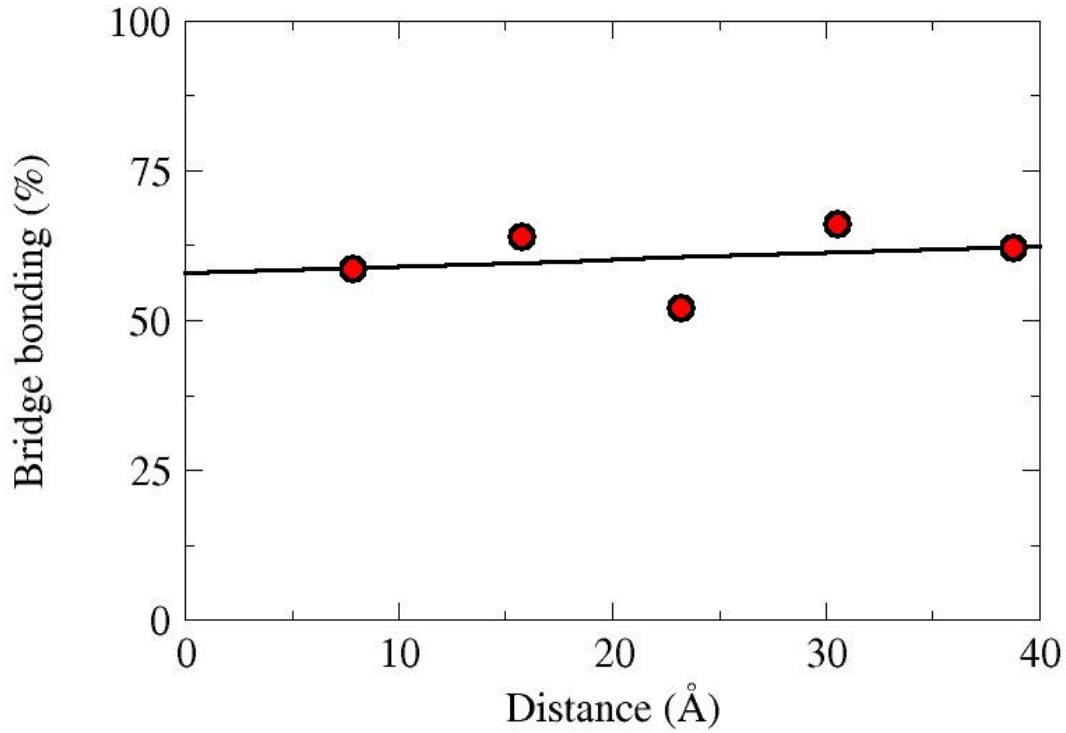

Fig. 3.6: Percentage of Si atoms taking part in a bridge bonde. The fluctuation over ~60% indicates no change with the variation of interparticle distance.

3.3.3 Oxygen percentage

Oxidation number is an analysis tool used to express the percentage of oxygen atoms in the system, namely it is the number of O atoms that a Si atom has. That means that oxidation numbers Si^{1+}, Si^{+2} and Si^{+3} correspond to the suboxides Si_2O, SiO and Si_2O_3respectively. In this way, it is obvious that the variation of the oxidation numbers would be from Si^{+0}, in the centre of the nc, to Si^{+4}, deep in the amorphous matrix.

It is known that in the ideal interface Si(100)/a-SiO_2 there exist only silicon atoms with oxidation number +2 (Si atoms with 2 oxygen as neighbors), while in the case of interface Si(111)/a-SiO_2 intermediate oxidation numbers, +1 or +3, are present as well. On the other hand, it is shown experimentally that in Si/SiO_2 there is a chemically nonabrupt interface with the coexistence of all intermediate oxidation

states. Examining more carefully the structure, it is found that there are distinct areas in which there are mainly one or two oxidation states. In our system we expect to have all the oxidation numbers at the surface because of the spherical shape of the nc. In order to affirm this, we calculated the oxidation distribution versus the distance from the centre of the nc, which is shown in Fig. 3.7. The 8x8x8 supercell is chosen. Indeed, the coexistence of all oxidation numbers is verified and ensures the roughness of our surface. Furthermore, one would want to conclude that the Si^{1+} and Si^{2+} moieties are located right at the interface, while the Si^{3+} ones are distributed within a nm from the interface. The same results are found in the case of flat interfaces. A straightforward definition of the interface can be given by taking the layer that contains silicon atoms in intermediate-oxidation states. From this figure we can also estimate the width of the surface. It is clearly shown that the thickness of the transition region (where all the oxidation states coexist) is of the order of 0.8 nm. Note that all the supercells have almost the same chemical composition, hence despite of giving as valuable information about the chemical composition of the system, the oxidation percentage does not provide as with any information about the decrease of energy with the variation of the interparticle distance.

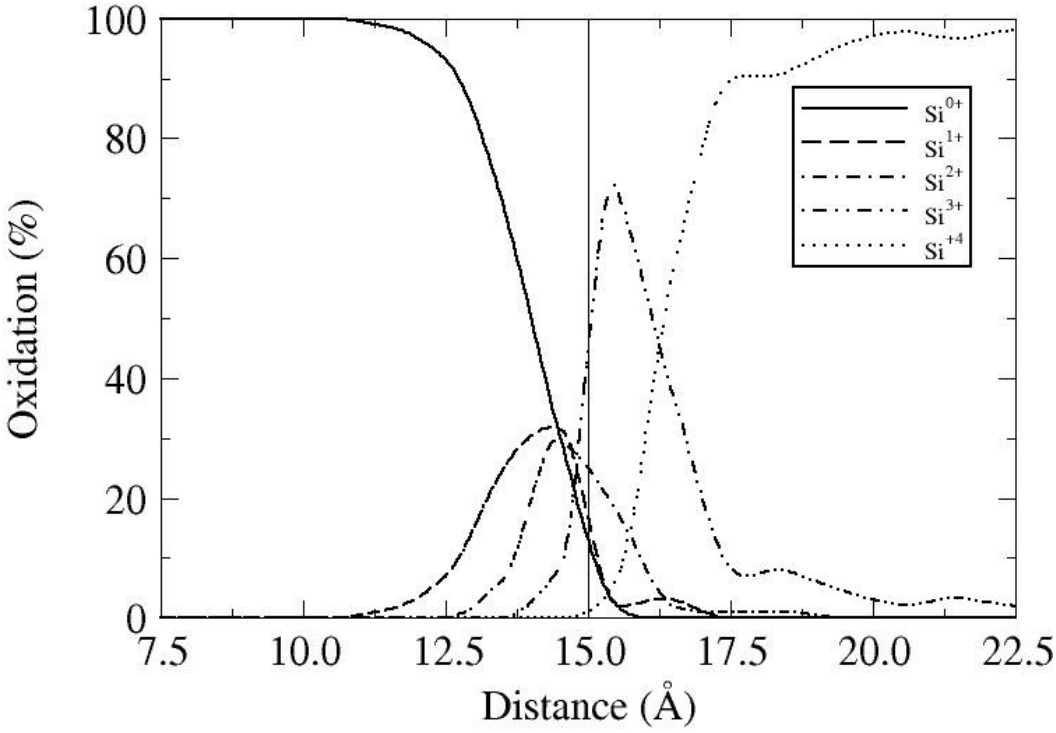

Fig. 3.7: Oxidation numbers versus the distance from the center of the nanocrystal, for the nc with d = 2.4nm. The vertical solid line shows the nominal position of the respective interface.

3.3.4 Tetrahedral Vector v_t

The tetrahedral vector (t_{vector}) is a measure of the networks disorder and deformation, namely v_t equals to the sum of the vectors pointing from an atom to it's nearest neighbours, and specifically shows the deviation from the ideal tetrahedral geometry (zero value). Thus, it includes both bond length and angle distortion. In our scenario the deformation revealed from t_{vector} does not seriously alter with the

variation of the interparicle distance. Nevertheless it is shown that when the distance is increasing the t_{vector} is slightely increasing as well. A representative graph of the t_{vector} versus the interparticle distance between the center of the nanocrystal till the boundary of the supercell is illustrated in figure 3.8.Three supercell are used.

We observe a progressive increase of deformation as the transition region is approached, and this is a consequence of embedding the nc in the host matrix. As we depart from the transition region the t_{vector} gradually decreases indicating more order in the matrix area.

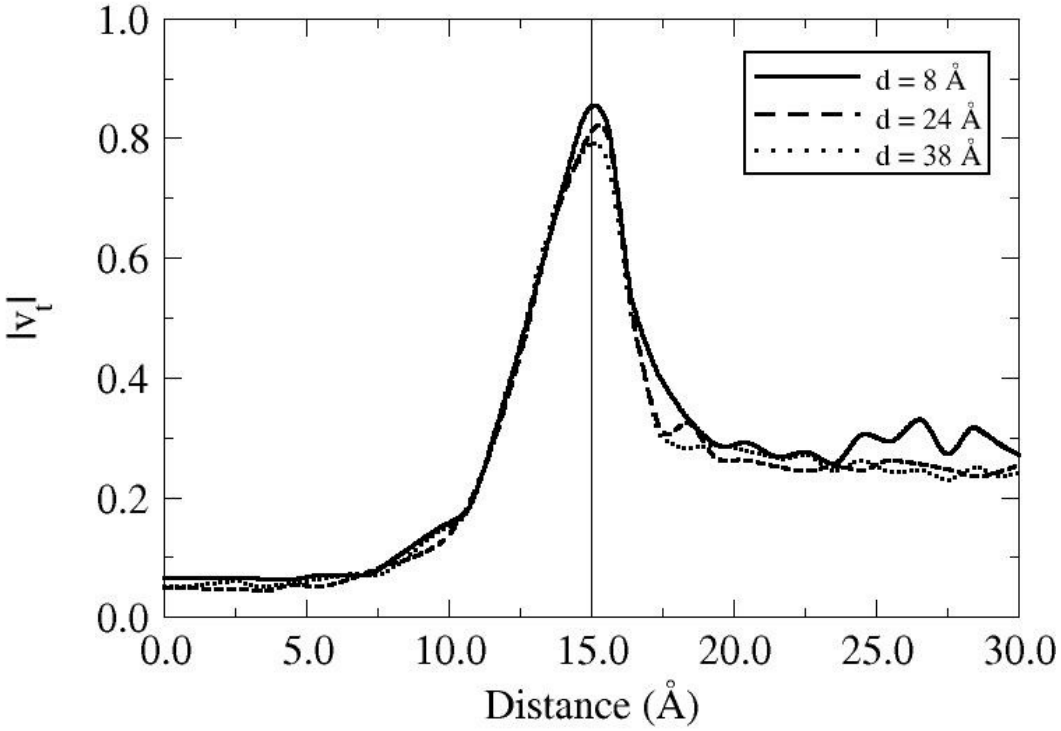

Fig. 3.8: The magnitude of the tetrahedral vector of three different nanocrystals versus the distance from their center. The vertical solid line shows the nominal position of the interface.

3.3.5 Decomposition of interface energy

The next step in our analysis is to examine, term by term the contributors in the formation energy. The latter is calculated via the Keating empirical potential in Eq. 2.5, in which the first two terms represent the cost of bond-length and bond-angle distortions, respectively, the third term is used to ensure that the neighbor list is preserved, and finally the term *U* represents a "suboxide penalty", the chemical energy cost to form any suboxide, taken by *ab initio* calculations. As it was referred to above a consequence of embedding the nc in the amorphous matrix is a highly strained cell. This strain energy is due to the mismatch of the Si-nc crystalline structure and the amorphous one of the matrix. The actual nature of the deformation and distortion is a deviation of the bonds between the atoms. This deviation has two aspects; the first is the deviation from the ideal bond length and the second is the deviation from the ideal bond angle. In fig.3.9 the line with the square points is the energy due to the bond length deviation and the line with the diamonds indicates the energy due to angle deviation, as a function of the interparticle distance. It is obvious that the distortion of angles is the dominant contributor in the energy, having a trend

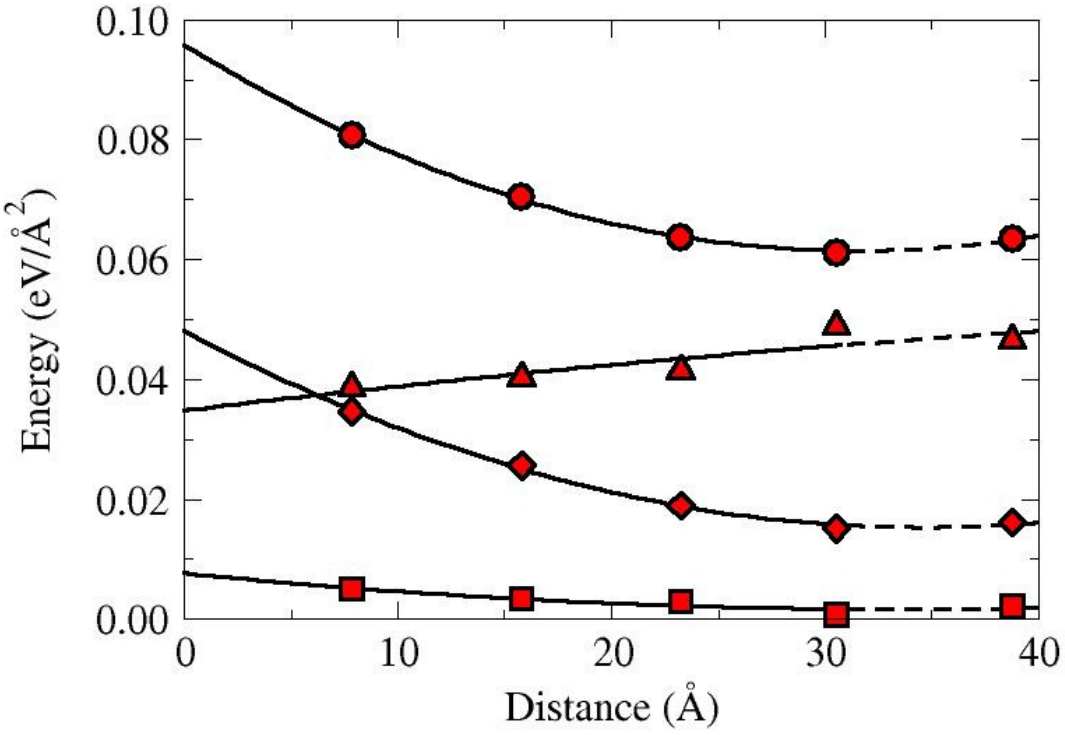

Fig. 3.9: Circular points indicates the total formation energy, square points is the energy due to the bond length deviation and the diamonds indicates the energy due to angle deviation .The triangle points indicates the "suboxide penalty".

much like the one of the total formation energy. The contribution from bond stretching also has the same trend, but it is much weaker.

On the other hand the contribution in energy coming from the suboxide atoms doesn't seem to follow the same trend with the total energy, moreover instead of decreasing with the expansion of the interparticle distance, increases. In order to examine the cause of the suboxides trend we decomposed their energy into atomic contributions and averaged over spherical shells. In this way we divided our cell into three regimes, the first starts from the centre of the core (zero point) with a width of 10Å showing in this way the contribution of the nc core to the strain energy, the second starts from the end of the latter and going up to 17Å, showing the contribution of the interface, and the third again starts from the end of the second and finishes on the boundary of the cell providing us with information about the contribution of the matrix to the strain energy. The results of this analysis are illustrated in Fig. 3.10. The line with the triangle points indicates the total suboxide energy, the line with the circular points indicates the energy of suboxide atoms in the second regime (interface) and finally the third regime (matrix) is indicated by the line with the square points.

The suboxides energy of the first regime does not appear in our figure because is almost impossible to have any oxygen penetration in the core. It clear that the biggest contribution in the suboxide energy comes from the interface area though the reason of the increase of suboxide energy lies in the contribution from the matrix. The actual reason for this increase emerges from the fact that in the matrix exist few Si^{3+} suboxides. This appearance of Si^{3+} in the matrix is due to the need in more time of the Monte Carlo method to extinguish all the coordination defects and fully relax the structure. Finally the more the atoms of the cell (in order to have greater interparticle distance) the more coordination defects will exist in the matrix.

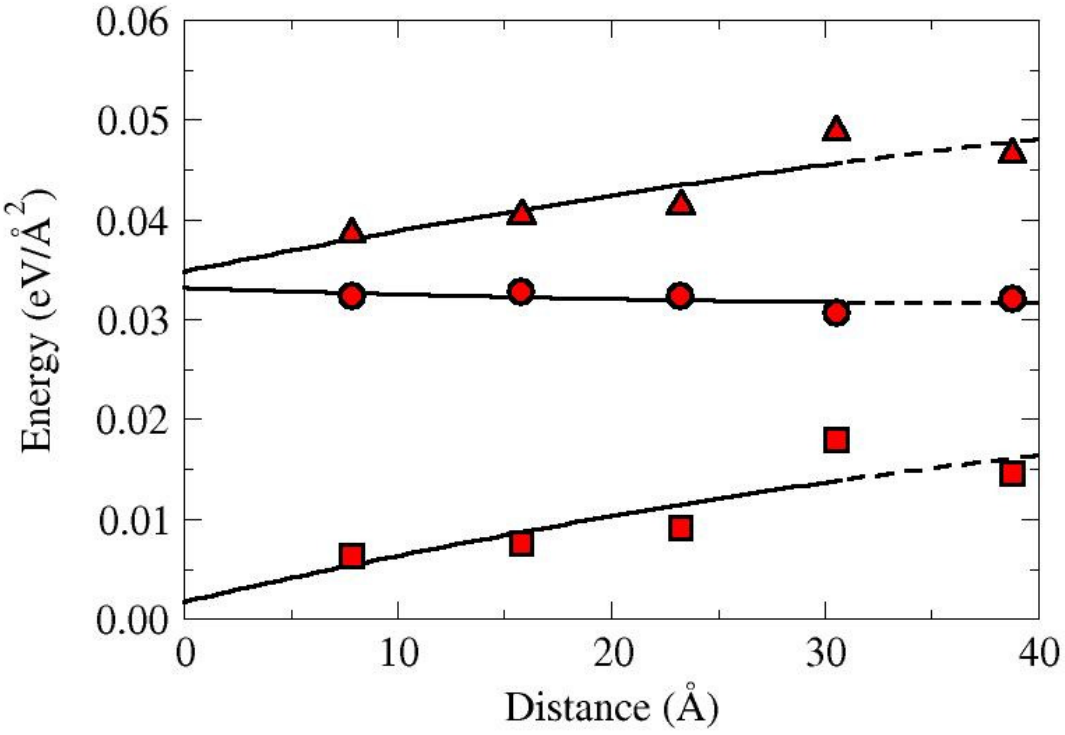

Fig. 3.10: The "suboxide penalty" decomposed into atomic contributions and averaged over spherical shells. Circular points indicate a shell with inner radius 10Å and 7Å width, square points indicate a shell with inner radius of 17Å and width till the end of the boundary, triangle points show the total suboxide energy.

As a final step, we decomposed the strain energy into atomic contributions and averaged over spherical shells. In this way we divided our cell into three regimes, same as the one of the suboxide analysis, i.e., the first starts from the centre of the core (zero point) with a width of 10 Å showing in this way the contribution of the core to the strain energy, the second starts from the end of the latter and going up to 17 Å, showing the contribution of the interface, and the third again starts from the end of the second and finishes on the boundary of the cell providing us with information about the contribution of the matrix to the strain energy. The strain energy per atom for the three regimes is illustrated in Fig. 3.12. The upper graph is for the first regime, the middle graph is for the second and the bottom graph indicates the third. We can easily see that the stain energy per atom of the core is low and without any real trend. On the other hand, the strain energy per atom in the interface and in the matrix clearly follow the trend of the formation energy. Interestingly, there seems to be a minimum in the variation of strain energy at the interface, which might be the reason for the minimum in the total energy. This can be explained as follows: when the nc's separate from each other at large distances, they become increasingly strained under the pressure exerted by the matrix. When they come too close, the interface is again strained due to the strong coupling of the strain fields between the nanocrystals. The optimum distance is achieved when the two strain fields, the one exerted by the matrix, and the other due to the coupling of the nc's, match each other.

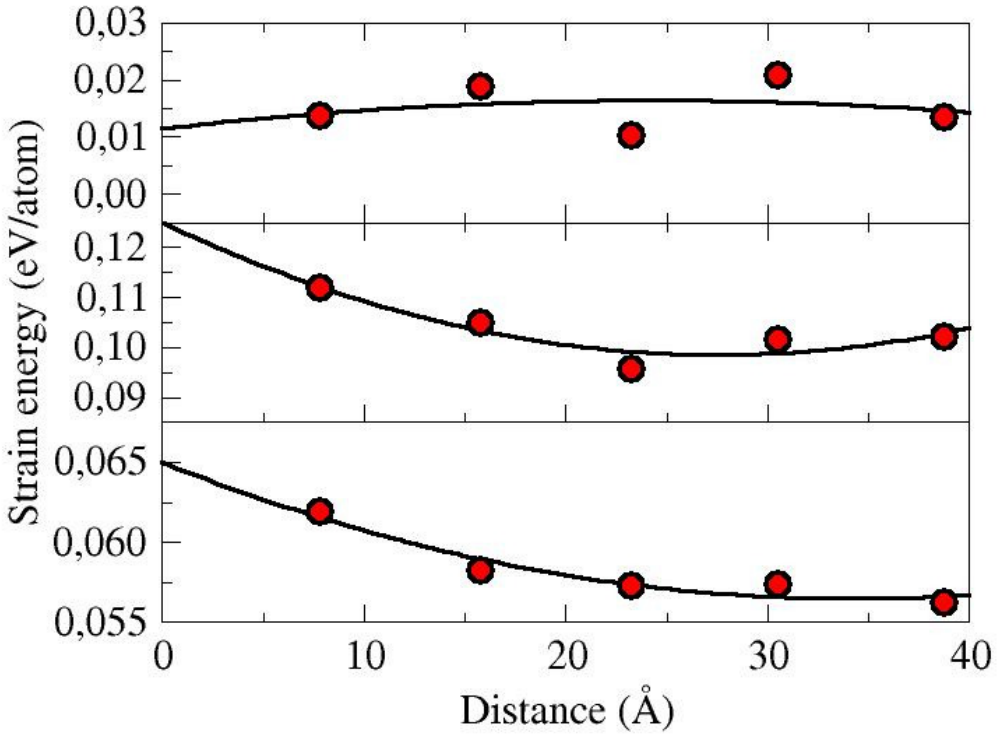

Fig. 3.11: The strain energy per atom of the in the core (upper graph), in the interface (middle graph) and in the matrix. (bottom graph).

3.4 Conclusion

In conclusion, we have shown that the interface properties of Si-nc are strongly influenced by the embedding amorphous oxide matrix, especially that the interfacial energy decreases with the variation of the interparticle distance, indicating higher stability of the entire nanocomposite system. Large deformations were observed, with the deviations in bond angles to be the dominant contributor to the strain energy. Our findings might play a crucial role in understanding and optimizing the PL properties of ordered Si-nc assemblies.

List of figures

2.9 Schematic representation of canonical ensemble. The number of particles, the volume and the temperature of the system are kept fixed, (N,V,T).

2.10 (a) supercell of crystalline silicon (c-Si) and its R.D.F. g(r) consisted of delta functions, **(b)** supercell of disordered system and its R.D.F. g(r) showing the special characteristics

3.1 Ball and stick model (part of a thin slice cut) of a Si-nc embedded in a-SiO2. Dark spheres show Si atoms in the nc. Large (small) grey spheres show Si (O) atoms in the oxide, respectively.

3.2 Si-nc cluster (a) generated via computational method (b) prepared in the lab.

3.3 Cubic cell in the beta-cristobalite structure. The cubic cell consists of 16 oxygen atom and 8 Si atoms.

3.4 Ball and stick model (part of a thin slice cut) of Si-nc embedded in a-SiO_2 cluster. The doted line denotes the boundaries of the supercell. The interparticle distance is simulated via periodic boundary condition.

3.5 The increase of the interparticle distance is followed by a decrease of the interface energy indicating higher stability of the system.

3.6 Percentage of Si atoms taking part in a bridge bonde. The fluctuation over ~60% indicates no change with the variation of interparticle distance.

3.7 Oxidation numbers versus the distance from the center of the nanocrystal, for the nc with d = 2.4nm. The vertical solid line shows the nominal position of the respective interface.

3.8 The magnitude of the tetrahedral vector of three different nanocrystals versus the distance from their center. The vertical solid line shows the nominal position of the interface.

3.9 Circular points indicates the total formation energy, square points is the energy due to the bond length deviation and the diamonds indicates the energy due to angle deviation .The triangle points indicates the “suboxide penalty”.

3.10 The “suboxide penalty” decomposed into atomic contributions and averaged over spherical shells. Circular points indicate a shell with inner radius 10Å and 7Å width, square points indicate a shell with inner radius of 17Å and width till the end of the boundary, triangle points show the total suboxide energy.

3.11 The strain energy per atom of the in the core (upper graph), in the interface (middle graph) and in the matrix. (bottom graph).

List of tables

Bibliography

[1] T. Shimizu-Iwayama, K. Fujita, S. Nakao, K.Saitoh, T. Fujita, and N. Itoh, *Visible photoluminescence in Si^+ -implanted silica glass*, J. Appl. Phys. **75**,7779 (1994).

[2] J. G. Zhu, C. W. White, J. D. Budai , S. P. Withrow, and Y. Chen, *Growth of Ge, Si, and SiGe nanocrystals in SiO_2, matrices*, J. Appl. Phys. **78**, 4386 (1995).

[3] K. S. Min, K. V. Shcheglov, C. M. Yang, H. A. Atwater, M. L. Brongersma, and A. Polman, *Defect-related versus excitonic visible light emission from ion beam synthesized Si nanocrystals in SiO_2*, Appl. Phys. Lett. **69**, 2033(1996)

[4] E. Werwa, A. A. Seraphim, L. A. Chiu, Chuxin Zhou, and K. D. Kolenbrander, *Synthesis and processing of silicon nanocrystallites using a pulsed laser ablation supersonic expansion*, Appl. Phys. Lett. **64,** 1821 (1994).

[5] L. N. Dinh, L. L. Chase, M. Balooch, L. J. Terminello, and F. Wooten, *Photoluminescence of oxidised silicon nanoclusters deposited on the basal plane of graphite*, Appl. Phys. Lett. **65**, 3111 (1994).

[6] H. Morisaki, F.W. Ping, H. Ono, and K. Yazawa*, Above-band-gap photoluminescence from Si fine particles with oxide shell*, J. Appl. Phys., **70,** 1869 (1991).

[7] S. Hayashi, T. Nagareda, Y. Kanzawa, and K. Yamamoto, Jpn. J. Appl. Phys., Part 1 **32**, 3840 (1993).

[8] Y. Kanzawa, T. Kageyama, S. Takeoka, M. Fujii, S. Hayashi, and K. Yamamoto, *Size-dependent near-infrared photoluminescence spectra of Si nanocrystals embedded in SiO_2 matrices*, Solid State Commun. **102**, 533 (1997).

[9] P. Melinon et al., Int. J. Mod. Phys. **9**, 339 (1995).

[10] F. Iacona, G. Franzo, and C. Spinella, *Correlation between luminescence and structural properties of Si nanocrystals*, J. Appl. Phys. **87,** 1295 (2000).

[11] T. Inokuma, Y. Wakayama, T. Muramoto, R. Aoki, Y. Kurata, and S. Hasegawa, *Optical properties of Si clusters and Si nanocrystallites in high-temperature annealed SiOx films*, J. Appl. Phys. **83**, 2228 (1998).

[12] C. Bonafos, B. Garrido, M. Lopez, A. Perez-Rodriguez, J. R. Morante, Y. Kihn,G. Ben Assayag, and A. Claveria, *An electron microscopy study of the growth of the Ge nanoparticles in SiO_2*, Appl. Phys. Lett. **76**, 3962 (2000).

[13] Y. Kanemitsu, T. Ogawa, K. Shiraishi, and K. Takeda*, Visible photoluminescence from oxidised Si nanometer-sized spheres: Exciton confinement on a spherical shell,* Phys. Rev. B **48,** 4883 (1993).

[14] H. Hofmeister, F. Huisken, and B. Kohn, Eur. Phys. J. D **9**, 137 (1999).

[15] A. Pasquarello, M.S. Hybertsen, and Car, *Interface structure between silicon and its oxide by first-principles molecular dynamics*, Nature (London) **396**, 58 (1998).

[16] K.O. Ng and D Vanderbilt, *Structure and oxidation kinetics of the Si(100)-SiO_2 interface*, Phys. Rev, B **59**, 10132 (1999).

[17] R. Buczko, S.J. Pennycook, and S.T. Pantelides, *Bonding Arrangements at the Si-SiO_2 and SiC-SiO_2 Interfaces and a Possible Origin of their Contrasting Properties*, Phys. Rev. Lett. **84**, 943 (2000).

[18] Y. Tu and J. Tersoff, *Microscopic Dynamics of Silicon Oxidation*, Phys. Rev. Lett. **89,** 086102 (2002).

[19] Y. Tu and J. Tersoff, *Structure and Energetics of the Si-SiO_2 Interface*, Phys. Rev. Lett. **84,** 4393 (2000).

[20] D. A. Luh, T. Miller, and T. C. Chiang, *Statistical Cross- Linking at the $Si_{(111)}$/SiO_2 Interface*, Phys. Rev. Lett. Bf 79, 3014 (1997).

[21] J.H. Oh et al., *Chemical structure of the ultrathin SiO_2/$Si_{(100)}$ interface : An Angle-resolved Si 2p photoemission study*, Phys. Rev. B **63**, 205310 (2001).

[22] A. A. Demkov, and O. F. Sankey, *Growth Study and Theoritical Investigation of The Ultrathin Oxide SiO2-Si Heterojunction*, Phys. Rev. Lett. **83**, 2038 (1999).

[23] R. J. Baierle, M. J. Caldas, E. Molinari and Stefano Ossicini, *Optical emission from small Si particles*, Solid State Commun. **102**, 545 (1997).

[24] M.V. Wolkin J. Jorne, P.M. Fauchet, G. Allan, and C. Delerue, *Electronic States and Luminescence in Porous Silicon Quantum Dots: The Role of Oxygen*, Phys. Rev. Lett. **82**, 197 (1999).

[25] A. Puzder, A. J. Williamson, J. C. Grossman, and G. Galli, *Surface Chemistry of Silicon Nanoclusters*, Phys. Rev. Lett. **88**, 097401 (2002).

[26] I. Vasiliev, J.R. Chelikowsky, and R. Martin, *Surface oxidation effects on the optical properties of silicon nanocrystals*, Phys. Rev. B **65**, 121302(R) (2002).

[27] N. Daldosso et al., *Role of the interface region on the optoelectronic properties of silicon nanocrystals embedded in SiO_2*, Phys. Rev. B **68**, 085327 (2003).

[28] G. Hadjisavvas and P. C. Kelires, *Structure and Energetics of Si Nanocrystals Embedded in a-SiO_2*, Phys. Rev. Lett. **93**, 226104 (2004); G. Hadjisavvas and P. C. Kelires, *Theory of interface structure, energetics, and electronic properties of embedded Si/a-SiO_2 nanocrystals,* Physica E (Amsterdam) **38**, 99 (2007).

[29] F. Djurabekova and K. Nordlund, *Atomistic simulation of the interface structure of Si nanocrystals embedded in amorphous silica,* Phys. Rev. B **77**, 115325 (2008).

[30] M. Ippolito, S. Meloni, and L. Colombo, *Interface structure and defects of silicon nanocrystals embedded into a-SiO_2,* Appl. Phys. Lett. **93,** 153109 (2008).

[31] F. Wooten, K. Winer, and D. Weaire, *Computer Generation of Structural Models of Amorphous Si and Ge*, Phys. Rev. Lett. **54**, 1392 (1985).

[32] P. N. Keating, *Effect of Invariance REuirements on the Elastic Strain Energy of Crystals with Application to the Diamond Structure*, Phys.Rev. **145**, 637 (1966).

[33] N. Metropolis, A. Rosenbluth, M. Rosenbluth, A. Teller, and E. Teller, *Equation of State Calculations by Fast Computing Machines*, J. Chem. Phys. **21**, 1087 (1953).

[34] G. T. Barkema, and N. Mousseau, *High-quality continues random networks*, Phys. Rev. B **62**, 4985 (2000).

[35] Yuhai Tu, J. Tersoff, G. Grinstein, and D. Vanderbilt, *Properties of a Continuous –Random-Network Model for Amorphous Systems*, Phys. Rev. Lett. **22**, 4899 (1998).

[36] D. R. Hamann, *Energetics of silicon suboxides*, Phys. Rev. B **61**, 9899 (2000).

[37] L.T. Canham, *Silicon quantum wire array fabrication by electrochemical and chemical dissolution of wafers*, Appl. Phys. Lett. **57**, 1046 (1990).

[38] L.W. Wang and Zunger, J. Phys. Chem. **98**, 2158 (1994).

[39] A.G. Gullis, L. T. Canham, and P.G.J. Calcott, *The structural and luminescence Properties of porous silicon,* J. Appl. Phys. **82**, 909 (1997).